

The ExtremeX global climate model experiment: Investigating thermodynamic and dynamic processes contributing to weather and climate extremes

Kathrin Wehrli¹, Fei Luo^{2,3}, Mathias Hauser¹, Hideo Shiogama⁴, Daisuke Tokuda⁵, Hyungjun Kim^{5,6,7}, Dim Coumou^{2,3}, Wilhelm May⁸, Philippe Le Sager³, Frank Selten³, Olivia Martius^{9,10,11}, Robert Vautard¹², and Sonia I. Seneviratne¹

¹Institute for Atmospheric and Climate Science, Department of Environmental Systems Science, ETH Zurich, Zurich, Switzerland

²Institute for Environmental Studies, VU University Amsterdam, Amsterdam, Netherlands

³Royal Netherlands Meteorological Institute (KNMI), De Bilt, Netherlands

⁴Center for Global Environmental Research, National Institute for Environmental Studies, Tsukuba, Japan

⁵Institute of Industrial Science, University of Tokyo, Tokyo, Japan

⁶Moon Soul Graduate School of Future Strategy, Korea Advanced Institute of Science and Technology, Daejeon, Korea

⁷Department of Civil and Environmental Engineering, Korea Advanced Institute of Science and Technology, Daejeon, Korea

⁸Centre for Environmental and Climate Science (CEC), Lund University, Lund, Sweden

⁹Oeschger Centre for Climate Change Research, University of Bern, Bern, Switzerland

¹⁰Institute of Geography, University of Bern, Bern, Switzerland

¹¹Mobiliar Lab for Natural Risks, University of Bern, Bern, Switzerland

¹²Institut Pierre Simon Laplace, Laboratoire des Sciences du Climat et de l'Environnement (LSCE), Gif sur Yvette, France

Correspondence: Kathrin Wehrli (kathrin.wehrli@env.ethz.ch)

Abstract. The mechanisms leading to the occurrence of extreme weather and climate events are varied and complex. They generally encompass a combination of ~~dynamical and thermodynamical~~ dynamic and thermodynamic processes, as well as drivers external to the climate system, such as anthropogenic greenhouse gas emissions and land-use change. Here we present the ExtremeX multi-model intercomparison experiment, which was designed to investigate the contribution of dynamic and thermodynamic processes to recent weather and climate extremes. The numerical experiments are performed with three Earth System Models: CESM, MIROC, and EC-Earth. They include control experiments with interactive atmosphere and land surface conditions, and experiments where either the atmospheric circulation, soil moisture or both are constrained using observation-based values. The temporal evolution and magnitude of temperature anomalies during heatwaves is well represented in the experiments with constrained atmosphere. However, the magnitude of mean climatological biases in temperature and precipitation are not ~~substantially~~ greatly reduced in any of the constrained experiments, ~~highlighting~~ due to persistent or newly introduced biases. This highlights the importance of error compensations and tuning in the standard model versions. ~~The results further~~ To show one possible application, ExtremeX is used to identify the main drivers of heatwaves and warm spells. The results reveal that both atmospheric circulation patterns and soil moisture conditions substantially contribute to the occurrence of ~~heat extremes~~ these events. Soil moisture effects are particularly important in the tropics, the monsoon areas and the Great Plains of the United States, whereas atmospheric circulation effects are major drivers in other mid- and high-latitude regions.

1 Introduction

Weather and climate extremes strongly affect society, human health, and ecosystems; therefore they need to be accurately simulated in numerical weather predictions and climate projections (e.g. Seneviratne et al., 2012). However, substantial biases remain in their representation in weather and climate models (e.g. Angélil et al., 2016; Maraun et al., 2017; Merz et al., 2020; Moon et al., 2018; Wehrli et al., 2018). ~~Aeross climate models of~~ For climate models used in the fifth phase of the Coupled Model Intercomparison Project (CMIP5), consistent biases can be found across models in the mean climatology of the lower atmosphere and land surface, for example temperature and precipitation (Flato et al., 2013; Mueller and Seneviratne, 2014). These biases originate to some extent from the representation of the underlying processes driving evapotranspiration at the land surface (Mueller and Seneviratne, 2014), extratropical cyclones (Zappa et al., 2013), or the simulated sea ice and sea surface temperatures (SSTs) (Turner et al., 2013; Wang et al., 2014a). The difficulties in representing the mean climatology translate to biases in the representation of extreme events and impede their projection into the future. Therefore, an important question in the investigation of changes in extremes in a warming climate is the identification of the respective contribution of thermodynamic (thermal structure, water vapor and precipitation, land-atmosphere interactions) and dynamic (large-scale circulation) processes to their changes in occurrence and intensity (e.g. Pfahl et al., 2017; Shepherd, 2014; Trenberth et al., 2015; Wehrli et al., 2018, 2019; Zappa et al., 2015). Better isolating these contributions would help inform further model development as well as research on the attribution and projection of changes in weather and climate extremes (Vautard et al., 2016).

In the past, the number of record-breaking hot extremes has increased and it is expected to increase further if anthropogenic emissions continue to rise (e.g. Rahmstorf and Coumou, 2011; Shiogama et al., 2016; Power and Delage, 2019). Changes in the frequency, intensity and duration of various types of extremes can be seen in different regions of the world (e.g. Seneviratne et al., 2012). The most extreme events show the highest sensitivity to climate change (Seneviratne et al., 2014; Sillmann et al., 2013) and new, ~~yet unseen, not yet seen~~ extreme intensities are appearing. These changes ~~follow from~~ are related to a number of physical processes, their interactions with each other and their response to climate change.

~~In~~ The processes driving a specific extreme event and their relative importance can be studied in observation-based studies using linear regression (e.g. Arblaster et al., 2014; Wang et al., 2016; Dirmeyer et al., 2021) or forecast sensitivity experiments (e.g. Hope et al., 2016; Petch et al., 2020). In climate model simulations the role of the drivers can be studied by constraining the processes in the ocean, the atmosphere or at the land surface, which enables the study of drivers in isolation (e.g. Fischer et al., 2007; Ha Recent work using these methods has shown that both soil moisture and atmospheric circulation play an important role in driving heatwaves (e.g. Dirmeyer et al., 2021; Petch et al., 2020; Suarez-Gutierrez et al., 2020). In this study, we present the new ~~"ExtremeX"~~ "ExtremeX" multi-model experiment in which, among other possible applications, the contribution of thermodynamic and dynamic processes to recent extreme events ~~is can be~~ investigated in three Earth System Models (ESMs). The models used in ExtremeX are the Community Earth System Model version 1.2 (CESM1.2), the Model for Interdisciplinary Research on Climate version 5 (MIROC5) and the European Community Earth System Model version 3 (EC-Earth3). The ~~ExtremeX~~ purpose of this study is (1) to introduce the ExtremeX experiments, and (2) to apply the introduced framework to

50 study the drivers of heatwaves and to identify globally for which locations warm spells are generally dominated by processes at the land surface or by atmospheric circulation.

~~The ExtremeX experiment builds on the study of Wehrli et al. (2019) and investigates the contribution of atmospheric circulation patterns vs. soil moisture conditions for extreme weather and climate events between 2010 to 2015. The experiments are and~~
55 recent climate change on extreme events. Therefore, experiments were carried out with prescribed (~~SSTs~~) SSTs and sea ice and additionally constraining the land surface and/or the atmosphere using observation-based conditions. ~~The atmospheric variability is Atmospheric variability was~~ constrained using a grid-point nudging approach (Jeuken et al., 1996) ~~, which relaxes the dynamical model variables toward a given meteorological field. Droughts and land-based heatwaves are often also associated to soil moisture scarcity, especially in transitional climate zones due to the strong land-atmosphere coupling (e.g. Seneviratne et al., 2010; Zscheischler and Seneviratne, 2017). To~~ to relax the horizontal winds toward reanalysis. This nudging approach has been verified for CESM in a further predecessor study (Wehrli et al., 2018) that also analysed biases for the nudged vs. non-nudged model climatologies, showing only minor changes to total biases. In Wehrli et al. (2019), soil moisture in the upper soil layers was constrained to control the role of land surface ~~feedbacks~~ feedback on extreme events; ~~soil moisture in the upper soil columns is constrained through either a nudging or a prescription method (depending on model implementation).~~
60 The experiments with atmospheric nudging and/or soil moisture prescription were then used to study recent heatwaves highlighting the combined role of dynamics (i.e. atmospheric circulation) and thermodynamics (in that case referring to land-atmosphere interactions) in driving these events.

Here, the same experiments are carried out for three ESMs. We introduce the experimental design and the three models composing ExtremeX and evaluate the constraining of the atmospheric circulation and land surface. Then the framework is
70 applied to investigate the contribution of atmospheric circulation patterns vs. soil moisture conditions for selected heatwaves between 2010 to 2015 and for the occurrence of warm spells. Other applications have not been tested so far and will be left to explore in future studies. The presented work expands on previous work in Wehrli et al. (2018, 2019) by ~~validating the forcing of the atmosphere and the land for the~~ quantifying biases of the near-surface climatology for different constraining experiments and three models. Near-surface temperature anomalies during four heatwaves evaluated in Wehrli et al. (2019) are compared
75 in the three ESMs of ExtremeX. Additionally, warm spells are examined grid-point wise to identify the role of the atmosphere and soil moisture for different spell lengths. The research questions asked in the following are:

- Are model deficiencies in atmospheric circulation and the land surface contributing to ~~overall~~ climatological model biases? Are model biases reduced when these processes are constrained?
- Are the ExtremeX ESMs able to reproduce temperature anomalies of past heatwaves when constrained with ~~observations~~ observation-
80 data?
- What is the role of the physical climate drivers and climate change for four observed heatwaves?
- What is the relative contribution of the land surface and the atmospheric circulation to warm spells globally and how do the contributions vary regionally?

Table 1. Overview of experiments and configuration of the model components. The ~~ensemble size~~ number of simulation runs for the experiments is given for the two successive simulation periods (# 1979–2008 and # 2009–2015/2016) ~~and for the models in the order: CESM1.2, EC-Earth3, MIROC5.~~

Name	Acronym	Atmosphere	Soil Moisture	Ocean	# 1979–2008	# 2009–2015/2016
Control	AI_SI	interactive	interactive	forced <u>prescribed</u>	<u>5, 5, 5</u>	100, <u>100, 100</u>
Soil moisture experiment	AI_SF	interactive	forced <u>prescribed</u>	forced <u>prescribed</u>	<u>5, 5, 5</u>	100, <u>100, 100</u>
Nudging experiment	AF_SI	forced <u>nudged</u>	interactive	forced <u>prescribed</u>	<u>5, 1, 5</u> ‡	<u>5, 1, 5</u> ‡
Fully constrained	AF_SF	forced <u>nudged</u>	forced <u>prescribed</u>	forced <u>prescribed</u>	<u>1, 1, 5</u> ‡	<u>1, 1, 5</u> ‡
Soil moisture climatology	AF_SC	forced <u>nudged</u>	forced <u>*prescribed*</u>	forced <u>prescribed</u>	<u>1, 1, 5</u> ‡	<u>1, 1, 5</u> ‡

* Soil moisture is ~~forced using~~ prescribed to the 1982–2008 climatology of the reconstructed soil moisture time series.

~~‡The modeling groups used different ensemble sizes for the experiments with constrained atmospheric variability. The numbers were constant over the 1979–2015/2016 period for the individual models.~~

2 Design of the model intercomparison project

85 The ExtremeX experiment was conducted in a collaboration of three modeling groups running three ESMs, whereof two (CESM and MIROC) were run in the CMIP5 configuration and one (EC-Earth) in the CMIP6 configuration. Five experiments were designed to ~~tackle~~ unravel the source of model biases and to separate the contribution of atmospheric circulation and land surface conditions to extreme events. This is done by constraining the ocean, land surface and atmosphere using observation-based values. The experiments and methods used are described in the following. ~~They, and~~ overall follow the setup of Wehrli et al. (2019).
90

2.1 Experimental design

Five experiments are included in ExtremeX. All experiments prescribe SSTs, sea ice and vegetation but differ in the simulation of the atmospheric circulation and soil moisture that are either interactive or ~~prescribed~~ constrained. See Table 1 for an overview of the experiments. The control experiment (AI_SI, “Atmosphere Interactive, Soil Interactive”) uses the standard setup where
95 the atmosphere and soil moisture are both interactive. In the soil moisture experiment (AI_SF, “Atmosphere Interactive, Soil Forced”) the atmosphere is interactive and soil moisture is ~~prescribed~~ constrained, and vice versa for the nudging experiment (AF_SI, “Atmosphere Forced, Soil Interactive”), where the latter is only used to validate the atmospheric nudging in this study. Finally, in the fully constrained (AF_SF, “Atmosphere Forced, Soil Forced”) and soil moisture climatology (AF_SC, “Atmosphere Forced, Soil Climatological”) experiments both components are ~~prescribed~~ constrained; once using time-varying
100 and once climatological soil moisture.

~~A small ensemble of one or five members is used to create a climatology for~~ For each experiment, ~~starting one or five simulations are initialized~~ in 1979. The ensembles for AI_SI and AI_SF are enlarged from 5 to 100 members for 2009–

2015/2016. As ExtremeX was initiated in 2017, no longer time horizon was proposed. The ensemble-size-number of simulation runs for the other experiments (AF_SI, AF_SC and AF_SF) is constant. ~~CESM has The small ensembles of five members for AF_SI and one member for the other experiments with nudged atmosphere. MIROC has five members for all atmosphere nudged experiments and EC-Earth has one. The small ensemble of MIROC and from MIROC and~~ CESM were used to verify that confirm that variability between the members is highly reduced for winds at the surface ~~are highly determined~~ by nudging the higher model levels, even though in the ExtremeX setup, winds are unconstrained in the lowest model levels (Sect. 2.2.1, see also Sect. 4 and Fig. A1). The analysis of the simulations starts in 1982 because the first three simulation years are regarded as spin-up. Likewise, 2009 is regarded as the spin-up for the additional members to diverge and therefore analysis of the years 2010–2015/2016 is recommended for example for event-based analysis of extremes, as is done here.

~~The models were forced with observed or reanalysis data~~ For the simulations, natural and anthropogenic forcing was used from observation-based products during the observational period and with from scenarios thereafter (Sect. 3). The three models choose different scenarios, either the Representative Concentration Pathway 8.5 (RCP8.5; van Vuuren et al., 2011) (CESM), RCP4.5 (MIROC) or the Shared Socio-economic Pathway 3-7.0 (SSP3-7.0; Meinshausen et al., 2020) (EC-Earth). The choice between RCP4.5, RCP8.5 and SSP3-7.0 is not expected to affect the results in this study as the scenarios barely differ for the considered time period.

2.2 Methods

The ocean, land surface and atmosphere are constrained to follow observation-based values, either time-varying or climatological ones. All experiments are conducted with SSTs and sea ice concentration prescribed. In the following, the methods to constrain the atmospheric circulation and the land surface are described. We use the ~~terms “forcing” and “constraining” interchangeably~~ term “constraining” as an umbrella term for the applied nudging ~~and prescription~~ of the atmospheric winds and/or large-scale circulation and the prescription of soil moisture.

2.2.1 ~~Constraining of atmospheric~~ Atmospheric circulation nudging

Nudging the atmospheric circulation in a climate model strongly reduces the dynamic variability in a simulation. For ExtremeX, all modeling groups use a grid-point nudging approach (Jeuken et al., 1996) to ~~force~~ constrain the atmospheric large-scale circulation by adding a tendency term to the prognostic equations of the zonal and the meridional ~~wind. This term~~ winds:

$$\frac{\partial U}{\partial t} = \dots - \frac{K(z)}{\tau} \left(U(x, t) - U_{target}(x, t) \right) \quad (1)$$

The term to the right hand side of Equation 1 is computed from the difference between a reference data set U_{target} and the computed model value (U). It is weighted by a relaxation time scale τ (Kooperman et al., 2012), which controls the strength of the constraint. A very short relaxation time scale means a strong constraint of the dynamics while a long relaxation time scale allows larger deviations from the reference. The length of the relaxation time scale is chosen such that it does not dominate

model physics but guarantees good agreement with the reference data set. All three models use a 6 h relaxation time scale following Kooperman et al. (2012). The reference data is given by 6-hourly wind fields from the ERA-Interim reanalysis (Dee et al., 2011), which are linearly interpolated to the model time step and regridded to the model resolution. At each model time step, the nudging term is used to update the horizontal wind variables. Additionally, a height-dependent weighting is introduced which allows $K(z)$ is introduced, enabling a free evolution of the boundary layer while nudging strength increases with height and controls the large-scale circulation (mostly above 700 hPa). The exact implementation of the height-dependent profile was chosen by the groups individually to fit their respective models (Fig. 1).

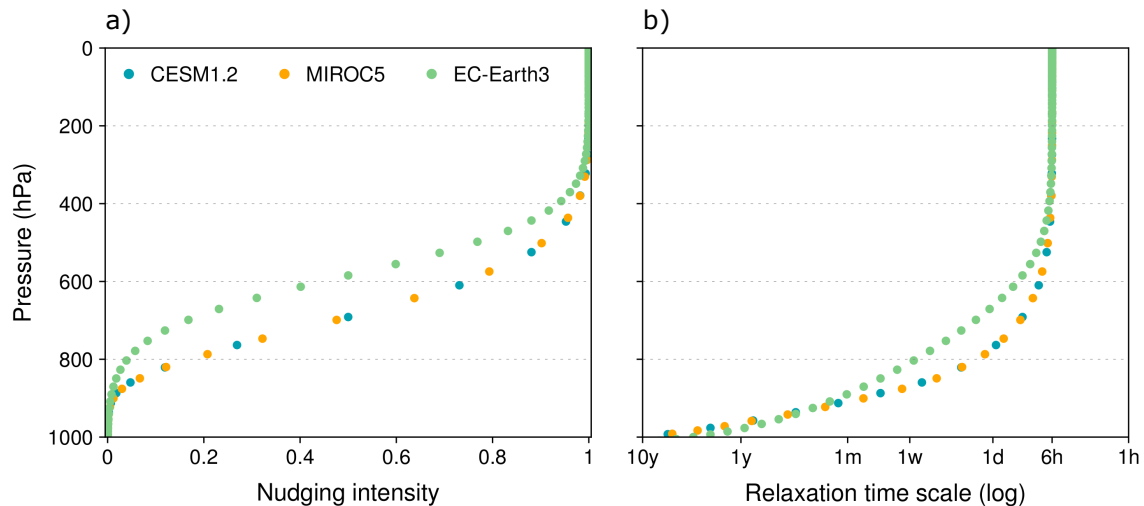


Figure 1. Nudging profile for the three ExtremeX ESMs. The actual pressure levels height-dependent nudging intensity ($K(z)$, a) and resulting relaxation time scale from the division by τ (b) are marked with an x and joined with lines/dots for each model. The nudging intensity is given from zero (no nudging) to one (fully nudged).

2.2.2 ~~Constraining of soil~~ Soil moisture prescription

Constraining Prescribing soil moisture in a climate model allows to isolate the enables the isolation of the main effects of land surface conditions and feedbacks on the feedback on climate. In an experiment with an unconstrained atmosphere interactive atmosphere but prescribed soil moisture (AI_SF), the circulation will adapt to the given land surface conditions, but there is no feedback in the opposite direction. Hence, the land is decoupled from the atmosphere. In the present set-up, soil moisture is forced prescribed to reflect observed conditions, similar to the SST-driven and nudged-circulation simulations. However, directly prescribing soil moisture from observations or observations-based products (e.g. reanalyses) in a climate model can lead to inconsistencies due to differences in model climatologies and soil parameterisations (Koster et al., 2009). Instead, observation-driven soil moisture reconstructions are generated by driving the land surface module of the respective ESM with observed meteorological observations meteorological fields from reanalysis data (e.g. air temperature, humidity, wind, precip-

itation, radiation). The generated daily or 6-hourly soil moisture constitutes the model-specific soil moisture reconstruction. This allows soil moisture in the ~~constrained-prescription~~ experiments to follow ~~observed-observed-based~~ soil moisture states, while still being in balance with the model climatologies and land model parameterisations. The method to constrain the land model with soil moisture reconstructions is inspired by the approach developed by Hauser et al. (2017b) for CESM. Not all
155 models followed the approach in every ~~respects~~aspect, as it was adapted to the respective model and tools available (see details in the individual model descriptions in Sect. 3). The common idea is that the model hydrology is active, but at the end of each time step the modelled soil moisture is replaced with ~~or nudged toward~~ the target soil moisture from the reconstruction.

2.3 Reference data sets

The atmospheric nudging is validated using winds from ERA-Interim (Dee et al., 2011) as reference. Monthly near-surface
160 temperature is retrieved at 0.5° resolution from the Climatic Research Unit, University of East Anglia (Harris et al., 2020), using version 4.03 of the data set (CRUTS in the following). Precipitation data at 0.5° resolution is obtained from the Global Precipitation Climatology Centre full data product version 2018 (GPCC-FD; Ziese et al., 2018) and at 0.1° resolution from the Multi-Source Weighted-Ensemble Precipitation data set, Version 2.2 (MSWEP; Beck et al., 2018). As reference for evapotranspiration the long, merged synthesis product (based on all data set categories) from the LandFlux-Eval data set at 1° horizontal
165 resolution is used (Mueller et al., 2013). Total cloud cover information was retrieved from the International Satellite Cloud Climatology Project D1 (ISCCP-D1; Rossow and Schiffer, 1999) at 2.5° resolution. All reference data sets are regridded to the original resolution of each model for the comparison.

2.4 ~~Data analysis~~Disentangling approach

In Sect. 5, we disentangle the contribution of the physical drivers (atmospheric circulation, land surface conditions and the
170 ocean state) and of recent climate change to temperature extremes. The method is briefly explained below, readers can refer to Wehrli et al. (2019) for more details. The disentangling method only takes anomalies of a variable with respect to the experiment climatology into account. In this study, the disentangling is applied to anomalies of daily mean temperature and daily maximum temperature (TX). The different contributions are assumed to be additive and, hence, differences between the experiments are computed ~~as shown in Fig. 2.~~

175 The fully constrained experiment (AF_SF) is taken as the “model truth” because it is as close to observations as the model can get. Therefore, AF_SF is set to 100 % of the event and the ~~analyses investigate~~ disentangling method determines what fraction of the event anomaly is explained by the other experiments. First, the contribution of recent climate change is computed as the anomaly of the years 2010–2015/2016 during the same time of the year the event took place (but excluding the event year) in AI_SI with respect to its 1982–2008 climatology. Note that a small fraction of the 2010–2015/2016 anomalies related to
180 the prescribed SST conditions, could also be due to decadal variability. The anomaly of AI_SI at a specific point in time (e.g. during an extreme event) compared to its 1982–2008 climatology is a combination of recent climate change (i.e. warming since the climatology period, which is estimated in the first step using the anomaly of non-event years from AI_SI), the observed SST pattern, and natural variability. The natural variability is controlled by using a large ensemble of 100 members. Hence,

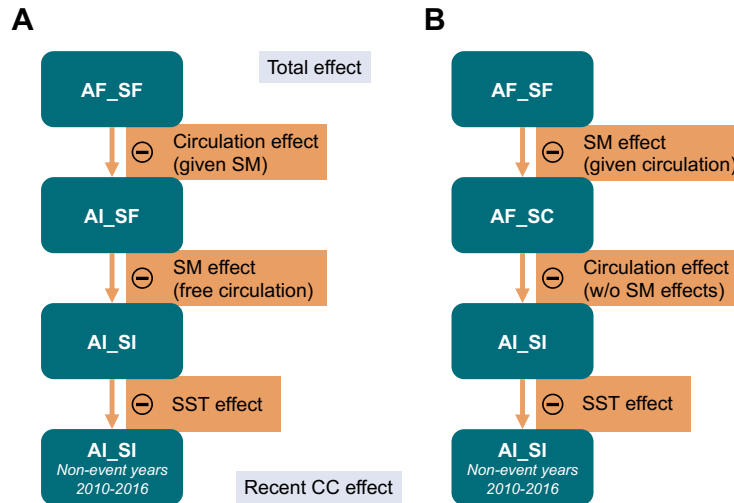


Figure 2. Schematic showing model experiments and effects isolated for temperature extreme events. For the experiments, the anomaly during the event (or during the same time of the year but for non-event years) is considered relative to the 1982–2008 climatology (turquoise rectangles). The magnitude of the anomaly in AF_SF is taken as the total effect and the anomaly of AI_SI during non-event years is taken as the recent climate change (CC) effect (grey boxes). Further effects are disentangled by computing differences between the experiments along the orange arrows as indicated by the minus sign (orange rectangles). Two approaches (black letters A and B) are followed differing in how soil moisture (SM) contributions are separated from atmospheric circulation contributions.

following the additive assumption, the remaining anomaly of AI_SI corresponds to the contribution of the ocean. To estimate
 185 the contribution of the land surface state (i.e. soil moisture) and the atmospheric circulation, the disentangling method by Wehrli
 et al. (2019) follows two approaches. The first approach (A) is to quantify the contribution of soil moisture as the anomaly in
 AI_SF minus the anomaly in AI_SI, and the contribution of the atmospheric circulation as the anomaly in AF_SF minus the
 anomaly in AI_SF. The second approach (B) is to quantify the contribution of soil moisture as the anomaly of AF_SF minus
 the anomaly of AF_SC, and the contribution of the atmospheric circulation as the anomaly of AF_SC minus the anomaly of
 190 AI_SI. Wehrli et al. (2019) show that the two approaches give similar results, which is confirmed here (Sect. 5). Hence, in this
 study the results from approaches A and B are averaged, giving equal weight to both. The results for the single approaches are
 also documented in the Appendix. The individual data analysis carried out for four recent heatwaves in Sect. 5.1 and warm
 spells in Sect. 5.2 is described in the respective sections.

3 Model descriptions

195 3.1 Community Earth System Model (CESM)

The Community Earth System Model is run in Version 1.2 (CESM1.2; Hurrell et al., 2013). Coupled are the Community Atmosphere Model Version 5.3 (CAM5; Neale et al., 2012) and the Community Land Model Version 4 (CLM4; Lawrence et al., 2011; Oleson et al., 2010). Both are run on a horizontal resolution of $0.9^\circ \times 1.25^\circ$. The atmosphere model, CAM5, uses hybrid sigma-pressure coordinates and has 30 vertical layers. CLM4 has 15 soil layers, whereof active hydrology is computed
200 in the upper 10 layers (down to 3.8 m).

Natural forcings as well as forcings from greenhouse gases (GHGs), aerosols and land-use change follow the setup in Wehrli et al. (2019). Major GHGs (CO₂, N₂O and CH₄) are prescribed to observed global values whereas other anthropogenic forcings follow RCP8.5 after 2005. A merged product of the Hadley Centre sea ice and SST data set Version 1 (HadISST1) and the NOAA weekly optimum interpolation SST analysis Version 2 (OI2) was used to prescribe transient monthly observations of
205 SSTs and sea ice concentrations (Hurrell et al., 2008). For ~~constraining soil moisture~~prescribing soil moisture, the prescription method developed by Hauser et al. (2017b) was used, which replaces the model-calculated soil moisture value by a target value at the end of each model time step. The ~~target data set~~prescribed target soil moisture is computed by running CLM4 offline ~~forced~~driven by reanalysis data from ERA-Interim. Below 0°C soil temperature in the model, soil moisture is computed interactively whereas at warmer temperatures the soil liquid water is prescribed to the total (liquid + ice) soil moisture of the
210 target data set. This prevents artificial creation of ice, which can produce unrealistic heat fluxes (Hauser et al., 2017b).

3.2 Model for Interdisciplinary Research on Climate version 5 (MIROC5)

The Model for Interdisciplinary Research on Climate version 5 (MIROC5) was developed jointly at the Atmosphere and Ocean Research Institute, University of Tokyo; National Institute for Environmental Studies; and Japan Agency for Marine-Earth Science and Technology (Watanabe et al., 2010). The horizontal spectral resolution of the model is T85 (wave number
215 85 with triangular truncation corresponding to a horizontal resolution of about 160 km). There are 40 vertical model levels of hybrid sigma-pressure coordinates up to 3 hPa. The land scheme of MIROC5 is an updated version of Minimal Advanced Treatments of Surface Interaction and Runoff (MATSIRO; Takata et al., 2003), which predicts the temperature and water in six soil layers down to a depth of 14 m, one canopy layer, and three snow layers. The SST and sea ice concentration data of HadISST1 were used (Rayner et al., 2003). See Shiogama et al. (2013) for the setup of natural (solar irradiance and volcanic
220 activity) and anthropogenic (GHGs; sulfate, black and organic carbon aerosols; ozone; land use land cover change) forcing agents. The anthropogenic forcing agents after 2005 were based on RCP4.5.

For ~~constraining~~prescribing soil moisture in MIROC5, the model replaces the calculated soil moisture with a ~~prescribed~~target value at the beginning of each model time step ~~to force the land state toward the reference~~. The prescribed target soil moisture was simulated by the land scheme in offline mode ~~using forcing data~~driven by atmospheric fields from ERA-Interim.
225 To remove negative values of liquid soil moisture content, the replacing procedure also limits ice content so that the total soil moisture does not exceed the prescribed one.

3.3 European Community Earth System Model Version 3 (EC-Earth3)

The European Community Earth System Model (EC-Earth3) is a ~~non-operational~~ climate model with the atmosphere component based on the European Centre for Medium-Range Weather Forecasts' (ECMWF) Integrated Forecasting System (IFS) and ~~the model~~ it is maintained by the EC-Earth consortium. Version 3.3.1 with IFS cycle cy36r4 was used for the ExtremeX experiments. The horizontal spectral resolution of the model is T255 (about 80 km), and there are 91 vertical model levels. The model has a hybrid ~~coordinate system combining both sigma coordinates and also~~ sigma/pressure coordinate system and a reduced Gaussian grid (N128). All experiments were produced with the SSP3-7.0 CMIP6 scenario and prescribed monthly ocean fields from the merged HadISST1 and NOAA OI2 data set with pre-applied SST/sea ice consistency checks (Hurrell et al., 2008). More information regarding the model can be obtained from www.ecmwf.int, www.ec-earth.org, and Döscher et al. (2021, in review) for greenhouse gases, aerosols and land-use prescribed in EC-Earth3.

For ~~constraining~~ prescribing soil moisture in EC-Earth, the simulated soil moisture is replaced by the respective target values for each of the four soil layers at the end of each model time step. As target values, 6-hourly soil moisture data from ERA-Interim/Land (Balsamo et al., 2015) were used. ERA-Interim/Land uses the H-TESEL land surface model (Balsamo et al., 2009) which has four soil layers, covering 0 cm–7 cm, 7 cm–28 cm, 28 cm–100 cm and 100 cm–255 cm of the soil.

4 Validation of the constrained atmosphere and soil moisture experiments

~~Atmospheric nudging forces the simulated horizontal winds toward observations.~~ In the setup used for this study, the atmospheric nudging is stronger in the upper atmosphere and close to zero at the surface (Fig. 1). Hence, it can be expected that the variability between ensemble members is strongly reduced, especially at higher atmospheric levels, and that the simulated winds closely follow the ~~observations~~ winds in ERA-Interim with increasing nudging strength. This is confirmed by evaluating the wind fields of the three models at the grid point level. For MIROC (and less visibly also for CESM; Fig. A1) there is some variability between the five members of the AF_SI ensemble at near-surface levels, whereas at 500 hPa and above all members are nearly identical and an almost exact representation of the reference. For EC-Earth, only one simulation of AF_SI was run. Although the nudging profile of EC-Earth is shifted to higher altitudes compared to the other two models (Fig. 1), the horizontal winds represent the reference equally well ~~for the selected pressure levels~~ (Fig. A1; see also Fig. A2). For all models ~~prescribing nudging~~ the large-scale atmospheric flow also has a strong control on near-surface winds.

In the following, the climatological model biases are compared between the experiments. First, regional and global RMSEs are examined in Sect. 4.1. Then, the sign and location of seasonal biases is discussed in Sect. 4.2.

4.1 Global and regional biases in surface temperature and precipitation

Intuitively, one might expect that biases with respect to observations are reduced when either soil moisture or atmospheric circulation or both are constrained. Near-surface temperature ~~for example,~~ for example, is driven by radiative processes and surface turbulent fluxes. The incoming radiation is related to the abundance, thickness and composition of clouds, which is

parameterized in the models and driven by weather systems (e.g. Bony et al., 2015). Surface turbulent fluxes are driven by soil moisture availability, which affects the partitioning in sensible and latent heat fluxes, especially in transitional climate regimes (e.g. Miralles et al., 2019; Santanello et al., 2018; Seneviratne et al., 2010). Similarly, precipitation is affected by both soil moisture and atmospheric circulation. The location and intensity of rainfall and snow is driven by the passage of low and high pressure systems as well as by soil moisture conditions (e.g. van der Ent et al., 2010; Guillod et al., 2015; Moon et al., 2019).

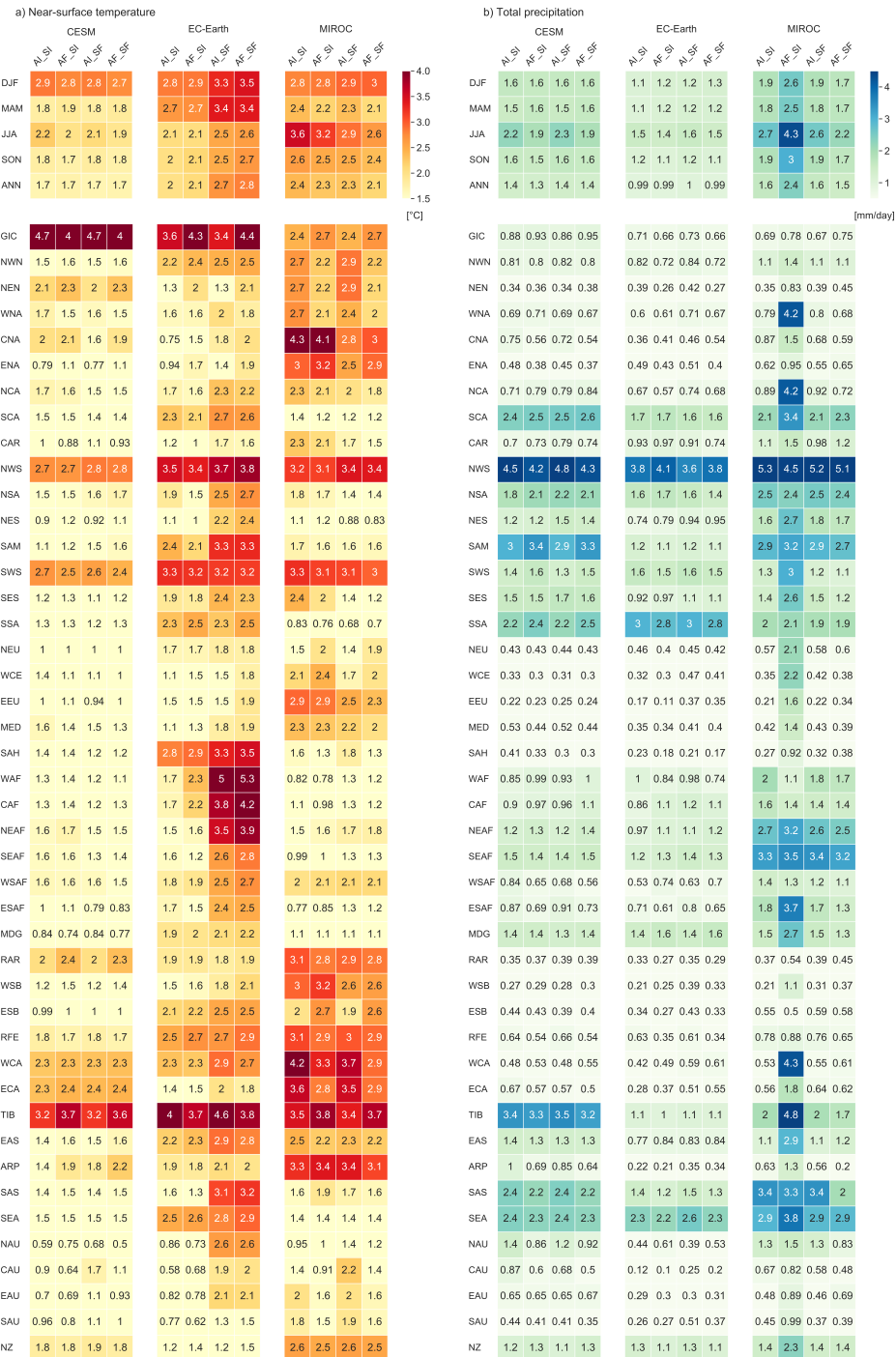
In the following, we quantify the near-surface temperature and precipitation biases in the experiments. Therefore, the model climatologies are compared to a reference by computing the root mean square errors (RMSEs) for the seasonal and annual averages of the 1982–2008 climatology. The mean over all simulation runs was computed where multiple members were available. Only land grid points are considered (except Antarctica).

In the global and annual average, the RMSEs in the experiments with ~~constrained-nudged~~ atmosphere and/~~or-or prescribed~~ soil moisture are nearly equal to the RMSE in AI_SI (Fig. 3). For EC-Earth the temperature bias increases when soil moisture is prescribed in AI_SF and AF_SF (Fig. 3a). For MIROC a large precipitation bias is introduced when nudging the atmospheric circulation in AF_SI (Fig. 3b). However, the bias is reduced in the fully ~~freed-constrained~~ experiment (AF_SF). Temperature biases are largest during the December-January-February (DJF) season in CESM and EC-Earth. In MIROC they are largest during the June-July-August (JJA) season, except for AF_SF where biases are largest in DJF. Precipitation biases are largest in JJA for all models. For the annual regional averages, large temperature biases can be found in regions with sparse observational coverage such as GIC (Greenland/ Iceland), NEN (northeastern North America) and RAR (Russian Arctic; Iturbide et al., 2020, for an overview of the AR6 reference regions see Fig. A3). Large temperature biases can also be found in small regions, which are only represented by a few grid points in the models used, such as NWS (northwestern South America), SWS (southwestern South America) and NZ (New Zealand). Additionally, the complex topography of the Himalayas (TIB) and Andes (SWS and NWS) is also a likely source of temperature biases. Regional precipitation biases are generally larger in wet regions such as the Amazonian regions SAM (South American Monsoon) and NSA (northern South America); and the regions in Central Africa, namely CAF (central Africa), SEAF (southeastern Africa) and NEAF (northeastern Africa); as well as the monsoon regions SEA (southeastern Asia) and SAS (southern Asia). Precipitation biases are also larger for small regions.

In general, the experiments with ~~constrained-nudged~~ atmosphere and/~~or-or prescribed~~ soil moisture do not show a significant reduction of the surface climatology RMSEs in any of the models or for any region of the world. In many cases, constraining the components of the model leads to even larger biases. This contradicts the initial intuitive assumption and suggests that no sole component of the model is responsible for the biases ~~and, hence, that these,~~ and hence the latter cannot be corrected in isolation.

4.2 Location and sign of seasonal biases

In the Northern Hemisphere mid-latitudes ~~the unconstrained,~~ the control simulations (AI_SI) for the CESM and MIROC models are systematically too hot (Fig. 4a) and in some regions also too dry (Fig. 5a) during boreal summer (JJA). North America, Central Asia and Eastern Europe show the largest biases. This agrees with the findings by Wehrli et al. (2018) for CESM. For EC-Earth, only Central Asia and parts of the Midwestern United States (U.S.) are too hot and dry, while other



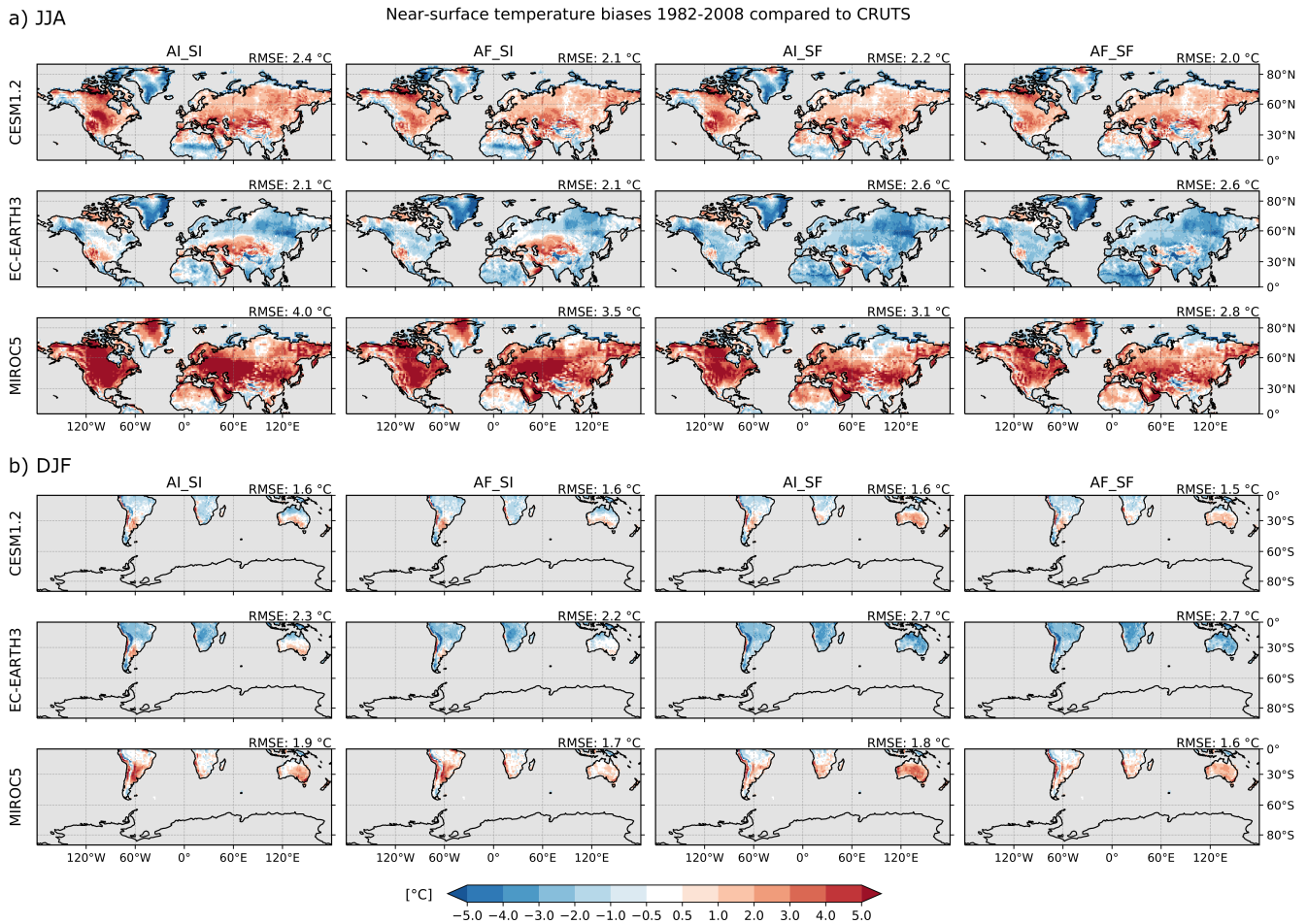


Figure 4. Bias in near-surface temperature (2m) with respect to CRUTS. Shown is the seasonal average over (a) June-July-August (JJA) for the Northern Hemisphere and (b) December-January-February (DJF) for the Southern Hemisphere. [Ocean grid points and Antarctica are masked out in grey.](#) The root mean square error (RMSE) averaged over all land grid points of the respective hemisphere is given in the upper right corner of each experiment and model.

regions are mostly too cold and wet. In all models, the regions where JJA temperature is overestimated coincide with regions where cloud coverage is underestimated (Fig. A4). Especially in MIROC, a large negative cloud cover bias can be found for the Northern Hemisphere midlatitudes. In MIROC, large areas in central and eastern North America, eastern Europe and Asia show a negative evapotranspiration bias as well (Fig. A5). In CESM and EC-Earth evapotranspiration is underestimated in central Asia and parts of western North America. This indicates that the warm temperature biases are related to underestimated evapotranspiration and cloud coverage in JJA.

295

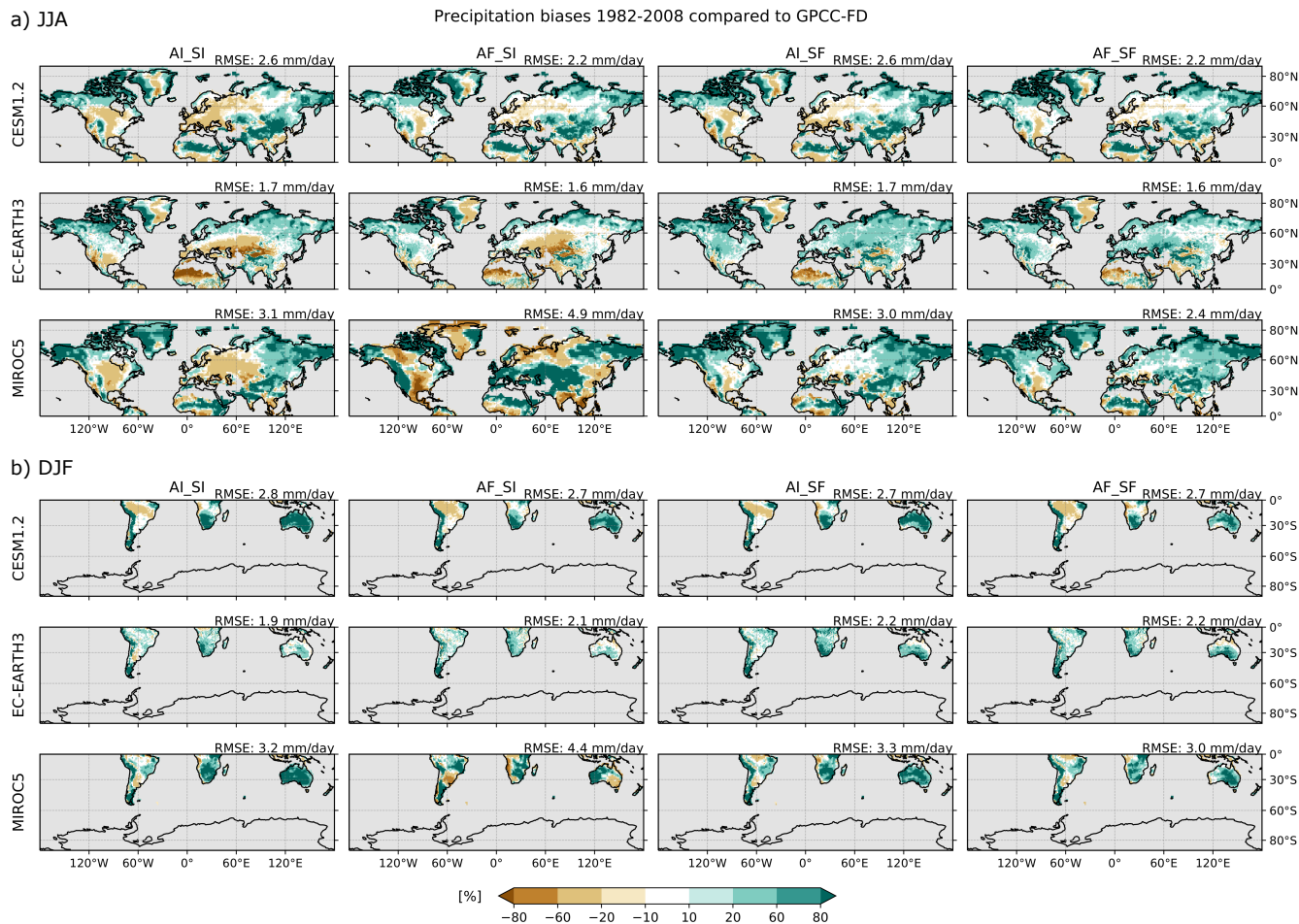


Figure 5. Bias in total precipitation with respect to GPCP-FD. Shown is the seasonal average over (a) JJA for the Northern Hemisphere and (b) DJF for the Southern Hemisphere. Values are given-plotted as percentage deviation from observationsthe reference data set. Same-Ocean grid points, Antarctica, as Figwell as grid points with a seasonal average of less than 0.1 mm precipitation per day in the reference data set are masked out in grey. -4 but-RSME-The RMSE averaged over all valid grid points of the respective hemisphere is given in mm per day in the upper right corner of each experiment and model.

Nudging the atmosphere in AF_SI reduces some of the JJA temperature biases in the Northern Hemisphere in CESM and MIROC (Fig. 4a). For MIROC, large precipitation biases are introduced with nudging (Fig. 5a). Some of the midlatitude regions change from too little precipitation to too much and vice versa. Hence, correcting the atmospheric circulation seems to lead to an overcompensation of biases in MIROC. In EC-Earth, nudging does not strongly affect the JJA temperature and precipitation climatology. Constraining the soil moisture in AI_SF leads to a reduction of the hot and dry bias in the Northern Hemisphere midlatitudes in MIROC. For CESM, the changes are smaller but there is a reduction of the hot and dry bias in Europe and the U.S. Midwest. For EC-Earth, constraining the soil moisture, however, introduces or increases the cold and dry bias nearly everywhere. The fully ~~freed~~-constrained experiment (AF_SF) is the experiment with the smallest temperature and precipitation biases for CESM and MIROC, suggesting that at least for these models, a correct representation of atmospheric circulation patterns and soil moisture conditions can improve the models' overall performance. Nonetheless, for EC-Earth AF_SF shows larger biases than AI_SI as the temperature biases introduced in AF_SF outweigh the biases corrected and similarly for precipitation, and for precipitation, the biases remain of similar magnitude.

The results for the austral summer (DJF) confirm the findings for the Northern Hemisphere in JJA. For EC-Earth, AI_SF introduces and increases a cold (Fig. 4b) and wet bias (Fig. 5b) in the entire Southern Hemisphere. MIROC shows large precipitation biases for AF_SI, which are (in certain places) of the opposite sign but similar or larger magnitude than in AI_SI. For CESM there are only very small differences between the experiments.

All models show substantial biases in total cloud cover fraction (Fig. A4) and evapotranspiration (Fig. A5), which match the biases found in temperature (e.g. negative cloud cover bias and negative evapotranspiration bias for areas that are too warm in the model) and sometimes also for precipitation. Both variables rely heavily on parameterisations. An alternative explanation for why biases are still prevalent after correcting the atmospheric flow and the land surface is that ESMs are tuned to match, e.g., the radiation balance at the top of the atmosphere and global mean values of variables like near-surface temperature, clouds or sea ice (Mauritsen et al., 2012). When single components of the models are constrained using more realistic fields from observational products, the model components are no longer in balance with each other. This can result in an overcompensation of biases, as can be seen for example for precipitation in MIROC (Fig. 5). It is known that MIROC5 shows biases in the North Atlantic storm track activity compared to ERA-Interim (e.g. Zappa et al., 2013). Correcting this circulation bias in AF_SI leads to even larger precipitation biases, which are only reduced when the soil moisture is constrained as well.

The seasonal precipitation climatology from the models was also compared to MSWEP (Fig. A6), confirming the above findings. The results for DJF for the Southern Hemisphere are very similar to the biases using GPCC-FD as reference. For JJA for the Northern Hemisphere, the models are more on the dry side when compared to MSWEP than if GPCC-FD is used as reference. The hemisphere-averaged RMSEs are in both cases very similar. Overall, the biases are not substantially reduced in any of the models when ~~constraining nudging~~ the atmospheric circulation ~~or~~ and/or prescribing soil moisture using observation-driven reconstructions. This shows that model biases are not primarily caused by the misrepresentation of large-scale atmospheric motion or soil moisture conditions. Instead, the biases might be caused by other processes such as radiation and cloud processes, convection, precipitation, as well as land surface properties (e.g. land cover and land use, topography) and processes unresolved due to the model grid scale such as mesoscale circulations and sub-grid surface heterogeneity. The

results also suggest that the models are tuned to have low temperature and precipitation biases in the interactive setup (with prescribed ocean).

335 5 Disentangling the contribution of physical drivers and climate change to recent heatwaves

In the previous section it was shown that large biases remain in the model climatology even if ~~observed-observation-based~~ conditions are used to constrain the models. Nevertheless, nudging the ~~atmospheric~~-large-scale ~~circulation and constraining~~ atmospheric circulation and prescribing the soil moisture results in simulations that can accurately reproduce the ~~observed~~ temporal evolution and relative magnitude of events. This was shown by Wehrli et al. (2019) using CESM for five recent
340 heatwaves, considering anomalies of TX. Hence, the presented set of experiments can be used to analyse extreme events if anomalies are used or a more elaborate bias-correction method is performed (e.g. Wehrli et al., 2020). In Sect. 5.1, four recent heatwaves are examined and it is shown that all three models accurately reproduce TX anomalies during and prior to heatwaves, when constrained with observation-based values. Then, the contribution of physical drivers and climate change is disentangled for the four heatwaves. The events chosen are: the 2010 Russian heatwave, the 2015 European heatwave, the
345 2012 heatwave in the ~~Midwest of the United States~~U.S. (also known as the Midwest heatwave), and the Australian heatwave of 2012/2013. All events had drastic consequences to the local communities and the economies due to e.g. damages to agriculture, wildfires and increased mortality. They were investigated in numerous previous studies including Wehrli et al. (2019). The events were chosen due to their severity and impact as well as to ensure consistency and comparability with Wehrli et al. (2019). In Sect. 5.2 warm spells (during the warm season) are analysed grid point-wise to identify the relative contribution of
350 atmospheric circulation vs. soil moisture.

5.1 Driving processes of recent heatwaves

For four heatwaves, the relative contributions of atmospheric circulation, soil moisture, ocean conditions and climate change (since 1982–2008) to TX anomalies are determined. As in Wehrli et al. (2019), spatial averages are taken over the event region and daily mean near-surface temperatures from ERA-Interim are used to identify the events. The hottest 15-day period defines
355 the event and TX during this period is examined. Ocean grid points are excluded from the analysis.

TX anomalies (with respect to 1982–2008) for the heatwaves and previous months are shown in Fig. 6. Overall, the fully ~~forced-constrained~~ experiments (AF_SF) from all models agree well with ~~observed-temperature anomalies~~ temperature anomalies from reanalysis and among each other. Small deviations are found during the 2010 Russian heatwave for MIROC, which underestimates the temperature anomaly (Fig. 6a), and during the 2012 ~~Midwest-U.S.~~ heatwave where CESM overestimates the temperature anomaly (Fig. 6c). TX anomalies for the same events from the nudging experiment (AF_SI) already compare well to ERA-Interim (Fig. A7) capturing the temporal evolution of TX anomalies similarly well as AF_SF. Correlation of near surface temperature anomalies between the experiments with atmospheric nudging and with ERA-Interim is very high. This confirms that observed surface anomalies can be accurately reproduced when nudging the atmospheric circulation. For

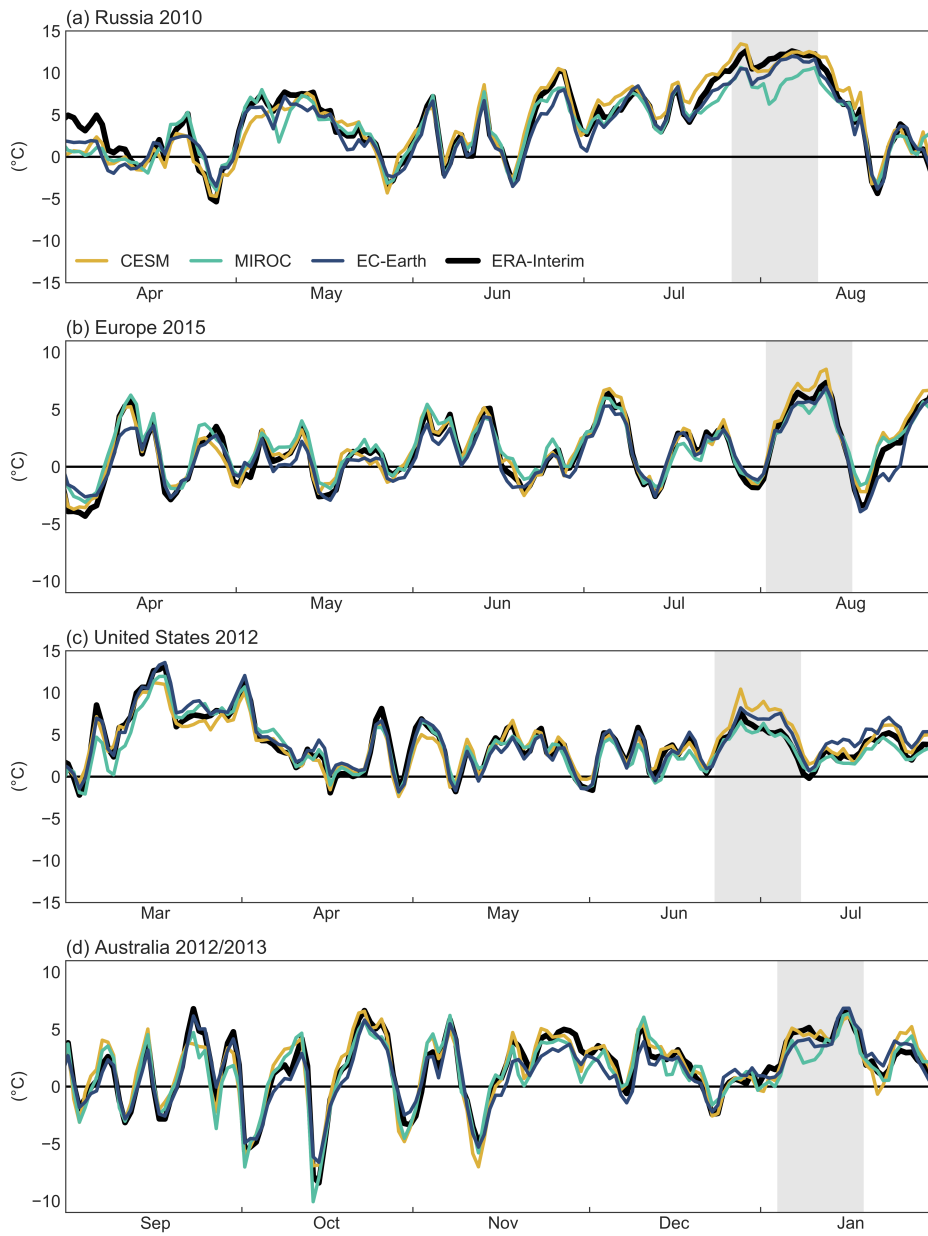


Figure 6. Daily maximum temperature anomaly compared to the 1982–2008 climatology for the fully forced-constrained (AF_SF) experiment for the three models and for ERA-Interim (black line). The 15-day event period is highlighted in light grey.

365 MIROC and CESM, which both have five AF_SI simulation runs, it can also be seen that nudging the atmosphere strongly
constrains variability between ensemble members (Fig. A7). In the following, the four heatwaves are analysed separately.

~~For the~~ The Russian heatwave of 2010 was characterized by extremely high temperatures over a long time period from late June to mid-August. A persistent blocking anticyclone was associated with the heatwave (e.g. Barriopedro et al., 2011; Trenberth and Fasullo 2011). Due to early snow melt in the year and a deficit of precipitation, water scarcity was exacerbating the heatwave (Barriopedro et al., 2011). For the analysis of the Russian heatwave of 2010, regional averages are computed over 50°N to 60°N and 35°E to 55°E ~~–(see Fig. A3 for the region outline).~~ The hottest 15-day period lasts from 27 July to 10 August 2010 (Fig. 6a). ~~Observed TX anomalies during the event~~ TX anomalies from ERA-Interim exceed 10°C during the event, which is captured well by CESM and EC-Earth. In MIROC the anomaly is somewhat weaker. In general, the three models agree on the contributions of the drivers to the TX anomaly (Fig. 7a). They estimate that recent climate change explains around 7%–10% of the event anomaly. CESM is the only model which shows a negative ocean contribution of around –7%, whereas the role of the ocean is negligible in the other models. ~~In~~ This result is supported by the studies by Dole et al. (2011) using initialized forecasts and Hauser et al. (2016) using an ESM which both found a weak role of the ocean. In contrast, observation-based studies like Martius et al. (2012) and Trenberth and Fasullo (2012) linked the driving atmospheric circulation conditions to SST anomalies identifying the ocean as an important driver. In all three models the event is mostly driven by atmospheric circulation and soil moisture, which agrees with existing literature. The ratio of the circulation contribution to the soil moisture contribution is 70:30 for EC-Earth and CESM and 80:20 for MIROC. Assessing the two approaches to disentangle atmospheric circulation from soil moisture contributions separately gives very similar results (Fig. A8a).

The European heatwave of 2015 consisted of four hot spells that were intensified by drought conditions through land-atmosphere feedbacks (Dong et al., 2016; Hauser et al., 2017a; Orth et al., 2016) The event is analysed over the Western and Central Europe (WCE) AR6 reference region (~~Hurtubeit et al., 2020, same as Central Europe (CEU) from previous assessment reports~~) (Hurtubeit et al., 2020). The hottest 15-day period is from 2 August to 16 August 2015 (Fig. 6b). The magnitude of the TX anomaly before and during the heatwave is represented well by all models. However, there are differences in the attribution of the drivers. In EC-Earth, climate change contributes around 12% to the event anomaly, whereas in CESM climate change is estimated to contribute 22% and in MIROC 34% (Fig. 7b). EC-Earth and CESM agree that there is a small negative contribution by the ocean of –9% and –7%, respectively. In MIROC the ocean is negligible for the event anomaly (around –1%). ~~The three~~ This is in contrast to the modeling study by Dong et al. (2016) and observation-based study by Duchez et al. (2016) finding that the SST patterns set important preconditions for the 2015 summer. The three ExtremeX models agree on the magnitude of the atmospheric circulation contribution, which is around half of the total event anomaly. However, the role of soil moisture depends on how much of the event anomaly is attributed to recent climate change. EC-Earth estimates the highest relative soil moisture contribution with a ratio of 60:40 between circulation and soil moisture. The ratio is 70:30 for CESM and 75:25 for MIROC. The results for the two disentangling approaches differ most notably for EC-Earth, where the ratios are ~~nearly balanced~~ 65:35 for one approach (~~B~~) and 65:35-A) but nearly balanced for the other (A); Fig A8b).

~~For the Midwest heatwave of~~ The U.S. heatwave 2012 evolved concurrently with a severe drought after an unusually warm winter and spring (Dole et al., 2014; Hoerling et al., 2014; Wang et al., 2014b). The event is assessed for the region from 35°N to 50°N and 55°W to 110°W ~~is assessed.~~The event is analysed from (see Fig. A3) and for 23 June to 7 July (Fig. 6c). The TX anomaly is represented well by MIROC and EC-Earth and a bit overestimated in CESM. The models agree well on the

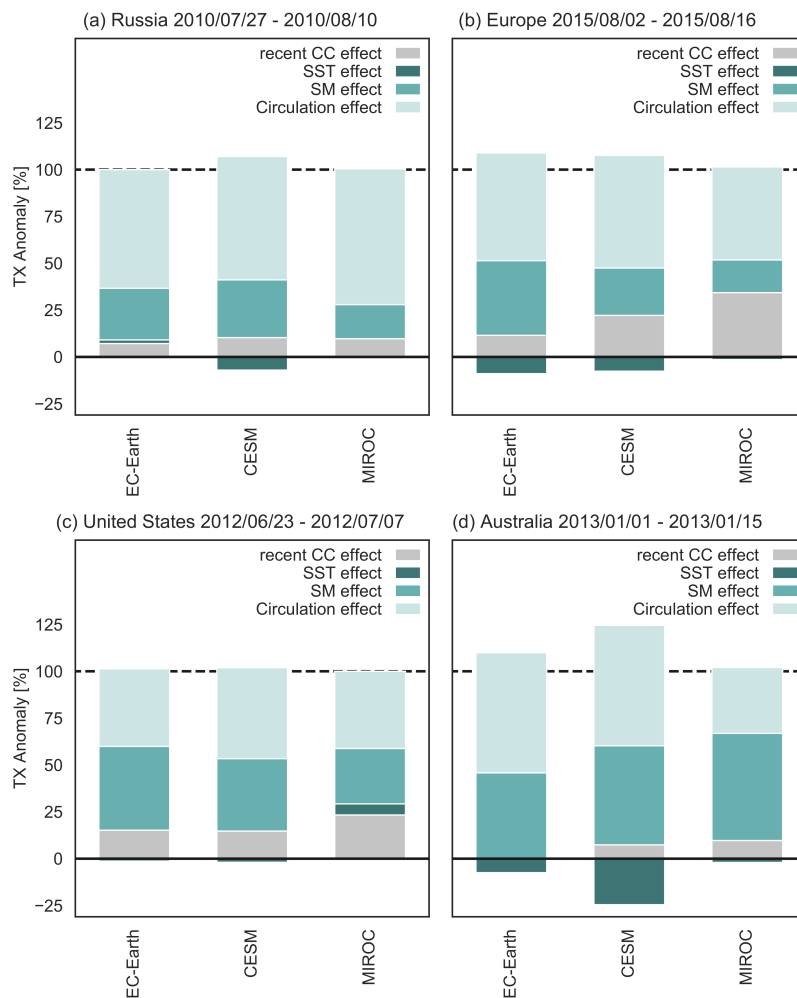


Figure 7. Contribution of recent climate change (since the 1982-2008 base period) and physical drivers to the daily maximum temperature (TX) anomaly during 4 recent events: a) Russia 2010, b) Europe 2015, c) ~~Midwestern U.S.~~ United States 2012, d) Australian summer 2012/2013. The dates of the hottest consecutive 15-day period are given in the label of each subplot. The contributions of the drivers are normalized by the climatology of AF_SF for each model, respectively. The two approaches to compute SM vs. ATM contribution are merged giving equal weight to both.

relative contribution of the drivers. In EC-Earth and CESM, recent climate change explains around 15% of the event anomaly, whereas for MIROC it is slightly more (23%, Fig. 7c). All models agree that the role of the ocean is very small, even if the sign is negative for EC-Earth and CESM (both -1%) but positive for MIROC (6%). [This agrees with Wang et al. \(2014b\) and Hoerling et al. \(2014\) who find the contribution by SSTs to be small.](#) The three models agree that the role of soil moisture conditions is about equal to the role of atmospheric circulation. [This is supported by earlier studies finding an important contribution by both the weather patterns and soil moisture deficit \(Hoerling et al., 2014; PaiMazumder and Done, 2016; Wang et al., 2014\)](#) The ratio of circulation to soil moisture contribution is 50:50 for EC-Earth, 55:45 for CESM and 60:40 for MIROC. The individual results for the disentangling approaches show that for all models soil moisture dominates for one approach (A) while atmospheric circulation dominates for the other (B); Fig. A8c).

405 [At its time, the summer of 2012/2013 was the warmest summer observed in Australia but it has since then been surpassed by the 2018/2019 and the 2019/2020 summers \(Bureau of Meteorology, 2020\).](#) The Australian heatwave of 2012/2013 is analysed for the region from 18°S to 30°S and 133°E to 147°E [\(see Fig. A3\).](#) The hottest consecutive 15-days occur just at the beginning of 2013 from 1 January to 15 January 2013 (Fig. 6d). The models represent the ~~observed TX anomaly~~ [TX anomaly from ERA-Interim](#) mostly well, except that in MIROC it is underestimated during the first half of the event period. While the contribution by recent climate change to the event anomaly is very small and negative in EC-Earth (-2%), CESM and MIROC agree on a small but positive contribution (7% and 10%, respectively, Fig. 7d). All models show a negative contribution of the ocean, which is most notable in CESM (around -25%), while in EC-Earth it is smaller (-7%) and almost negligible in MIROC (-2%). [This is in line with the La Niña conditions that established in 2010 and 2011 and transitioned to cool to neutral during the summer 2012/2013 \(NOAA Climate Prediction Center, 2022\) as well as with the findings by Lewis and Karoly \(2013\).](#) For EC-Earth and CESM the contribution by the atmospheric circulation is larger than by soil moisture, whereas for MIROC it is the other way around. [It was also found by King et al. \(2014\) that the dry conditions were an important driver of the heatwave.](#) The ratio of atmospheric circulation contribution to soil moisture contribution is 60:40 for EC-Earth, 55:45 for CESM and 40:60 for MIROC. For MIROC, the individual ratios from the two disentangling approaches ~~are similar and~~ both agree that the contribution of soil moisture is larger than the contribution of the atmospheric circulation to the event anomaly [whereas for the other two models the individual ratios are balanced to slightly circulation-dominated \(Fig. A8d\).](#) [This may reflect that the warm bias simulated by MIROC is alleviated significantly with soil-moisture constrained experiment \(Fig. 4\).](#)

420 Overall, the three models ~~agree well~~ [mostly agree](#) on the relative contribution of atmospheric circulation vs. soil moisture to the TX anomaly during four recent heatwaves. For the heatwaves of 2010 in Russia and 2015 in Europe, all models show that the atmospheric circulation plays the most important role. For the ~~Midwest-U.S.~~ [heatwave 2012,](#) the models agree ~~;~~ that soil moisture conditions are about as important as atmospheric circulation for driving the TX anomaly. For the Australian heatwave of 2012/2013, two models show that atmospheric circulation is more important whereas one model shows that the soil moisture contribution was largest. All models agree on a small role of climate change in driving the TX anomaly during the 2010 Russian heatwave and the 2012/2013 heatwave in Australia. However, for the 2015 European heatwave and the ~~Midwestern-U.S.~~ [heatwave in 2012,](#) the role of climate change differs between the models, being largest for MIROC and smallest for EC-Earth. The role of the ocean is small for the heatwaves of 2010 in Russia, 2015 in Europe and 2012 in the

Midwest,U.S. For the 2012/2013 heatwave in Australia, all models agree that the role of the ocean is negative – thus not favoring a heatwave – however, the models disagree on the magnitude, with CESM being the only model displaying a notable contribution by the ocean.

5.2 Relative contribution of atmospheric circulation and soil moisture to episodes of anomalously warm temperatures

440 In the following, we analyse the role of atmospheric circulation and soil moisture in driving the occurrence of warm spells during 1982–2015/2016 (2015 for MIROC and 2016 for the other two models). The disentangling method is the same as used previously in Sect. 5.1. Warm spells are defined grid point-wise as time periods during the local summer season where daily mean temperature anomalies in ERA-Interim exceed 1.5 standard deviations of the 1982–2010 climatology for at least three consecutive days. A 7-day running mean is applied to the years 1982–2010 from ERA-Interim before computing the
445 daily climatology and standard deviation. The local summer season is defined as the three hottest consecutive months (from ERA-Interim for each grid point). The threshold of 1.5 standard deviations was chosen such that most regions of the world actually experience events. However, using 1 or 2 standard deviations as threshold leads to very similar results (not shown). The identified warm spells are categorised into events of 3–5 days, 6–13 days and 14 days and longer. The spells choice of categories was made to separate events lasting a few days from week-long events and very long-lasting events of two weeks and more.
450 Also, the choice was made to obtain a reasonable sampling size for each category. The warm spells based on ERA-Interim are analysed by taking the same dates (calendar year and days of the year) in the experiments. First, the same dates are analysed for the fully constrained (AF_SF) experiment to determine the “model truth” for each event and model (using the ensemble mean for MIROC, which has five simulation runs). Then, the contribution of the drivers is disentangled according to Fig. 2. One or five ~~ensemble members~~ simulation runs (over the years 1982–2015/2016) are used, depending on how many were available
455 per model and experiment. The mean temperature anomaly of each event category and experiment (averaged over all events and simulation runs) is used to disentangle the relative contribution of the atmospheric circulation and soil moisture conditions grid point-wise.

The agreement among models is very high for all spell lengths (Fig. 8). The grid points where soil moisture contributes one third or more to the warm spells, agree well with the regions of high soil moisture-temperature coupling (Koster et al., 2004;
460 Miralles et al., 2012). With increasing spell length, the contribution of soil moisture becomes more important, for example in the U.S. Midwest, Eurasia and northern Australia. Further, with longer spell length there is a growing proportion of total soil moisture contribution as can be seen by the increasing percentage of soil moisture dominance for all models in Fig. 8. This shows the growing relative importance of the land surface state for long-duration events.

The analysis also reveals that warm spells of 14 days and longer with a magnitude of more than 1.5 standard deviation do
465 not occur often or in many regions of the world. The result for eastern Europe, for example, can be traced back to the Russian heatwave in 2010. For ~~regions that see perennial ice and permafrost, like Greenland or Siberia~~ tropical regions like Amazonia or very dry regions like the Sahara, it is not always possible to disentangle the relative contributions of atmosphere and soil moisture. ~~But also for Amazonia the contributions cannot be disentangled. This is because differences are computed that~~ This occurs because the computed differences can become negative if the less constrained experiments have a higher temperature

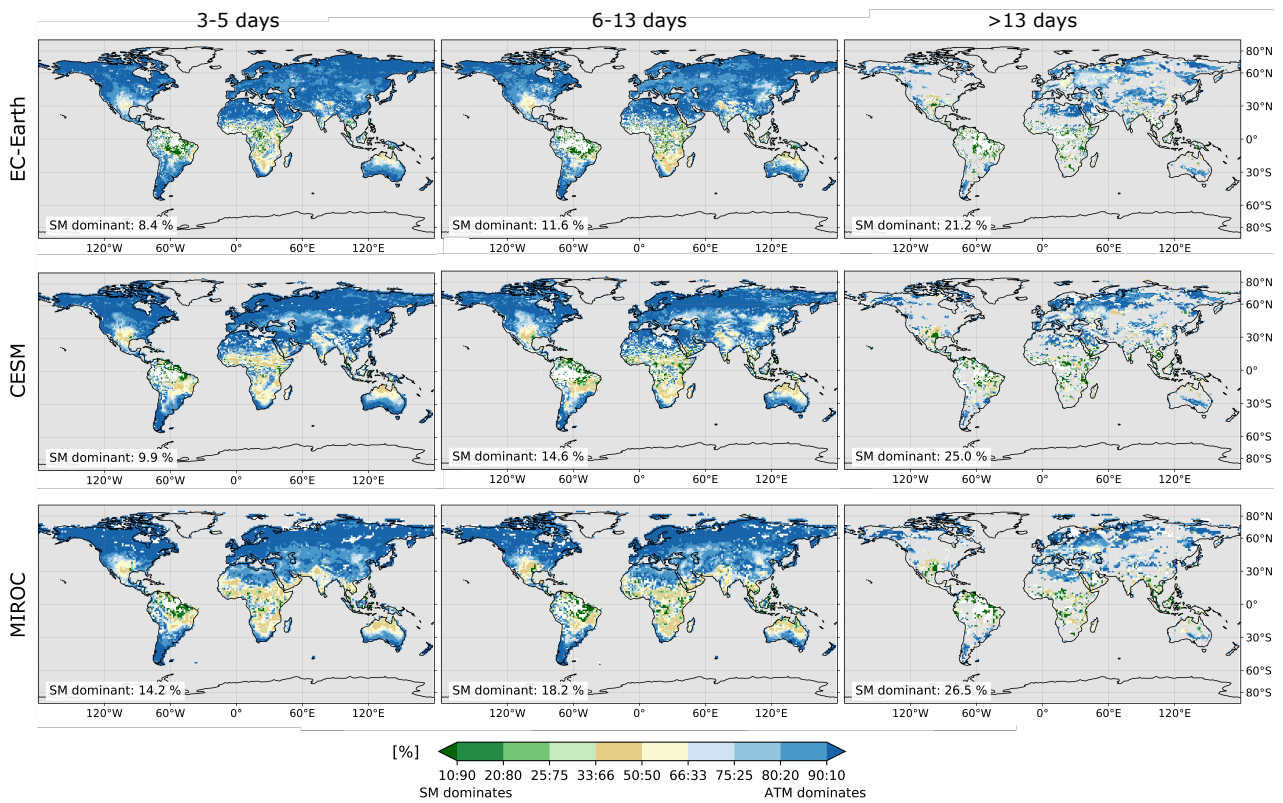


Figure 8. Contribution of atmospheric circulation (ATM) vs. soil moisture (SM) to warm spells during the local summer season where daily mean temperature anomalies exceed 1.5 standard deviation from the ERA-Interim 1981–2010 climatology. The local summer season is defined as the hottest consecutive three months (from ERA-Interim) for each grid point. The two approaches to compute SM vs. ATM contribution are merged giving equal weight to both. Events are categorised into spells lasting 3–5 days, 6–13 days and 14 days and longer. Ocean grid points, Antarctica, Greenland and Iceland are masked out in grey using the Greenland/Iceland (“GIC”) region from the AR6 reference regions for the latter two. Grid points where no events were identified ~~or~~ are also masked out in grey. Grid points where the contributions could not be determined (see text) are masked out in ~~grey together~~ white. In the lower left corner the grid points where the SM contribution dominates over the ATM contribution (>50%) are given as area-weighted percentage with ~~ocean~~-respect to all valid grid points.

470 anomaly than the more constrained experiments on average. The affected grid cells are masked out in ~~grey-together-with-ocean~~
~~grid-points~~ white in Fig. 8.

It has to be noted, that the analysis method takes into account the temporal persistence of warm spells but not temporal
correlation as for example the time-lagged effect of dry springs on hot summers (e.g. Hirschi et al., 2011; Quesada et al.,
2012). Furthermore, the events are only identified grid-point wise and not as spatially coherent patterns, as they would occur
475 naturally. This is responsible for some of the noise in the patterns.

6 Conclusions and outlook

The ExtremeX experiment is a multi-model intercomparison project designed to study processes contributing to the occur-
rence and intensity of extreme events. ExtremeX currently consists of simulations with three ESMs: EC-Earth3, MIROC5 and
CESM1.2. Five experiments with varying levels of ~~forcing-constraining~~ were run with all models. A grid-point nudging ap-
480 proach is used to constrain the modeled horizontal winds in the atmosphere and soil moisture ~~nudging-or~~ prescription is used
to constrain the land surface.

Although the constrained experiments ~~allow-to-capture-well~~ capture the temporal evolution and magnitude of temperature
anomalies well during recent heatwave events, climatological biases in temperature and precipitation remain in the experiments.
This is the case both for experiments with either ~~observationally-constrained-nudged~~ atmospheric circulation patterns and/~~or-or~~
485 ~~prescribed~~ soil moisture conditions. In some cases, even larger biases appear in the constrained experiments (Fig. 3). Comparing
the location and magnitude of the climatological biases reveals that the patterns and sign of the biases often remain and the
magnitude is only marginally reduced. This agrees with findings by Wehrli et al. (2018) for atmospheric nudging in CESM.
The results suggest that the biases are caused by other processes such as cloud and precipitation formation, convection and
interactions of the land surface and the ocean with the atmosphere, or also land surface parameters. It is also likely that none of
490 these other elements is the sole explanation for the climatological biases, but rather their interaction, including with atmospheric
circulation and soil moisture dynamics.

Despite the biases in mean climatology, the experiments with constrained atmosphere and soil moisture can accurately
reproduce ~~observed~~ temperature anomalies during and prior to heatwaves (Fig. 6). This is found for all models and sup-
ports the results by Wehrli et al. (2019) for CESM. ~~Thus, the~~ This result implies that alternatively bias correction could be
495 used to improve the representation of extreme events in the models instead of analysing anomalies as is done here. The pre-
sented set of experiments can be used for extreme event analysis as long as the atmospheric circulation and/or soil moisture
are major drivers of the event. The ~~result also implies that bias correction could be used to improve the representation of~~
~~observed extreme events instead of analysing anomalies.~~ experiments are not ideal if the focus is on the role of the ocean,
because the ocean is prescribed. For events that are mainly ocean-driven, we would recommend a setup with interactive
500 ocean experiments to compute the ocean contribution more accurately. Nevertheless, here we derive the approximate ocean
contribution by comparing the anomaly to non-event years. The present study disentangles the role of atmospheric circula-
tion vs. land surface processes for temperature anomalies. Therefore, additivity of the different contributions is assumed. This

is inspired by the study by Kröner et al. (2017) for summer climate in Europe. Following the disentangling in Wehrli et al. (2019), experiments with constrained soil moisture (AI_SF) and with nudged atmosphere and soil moisture constrained to climatological values (AF_SC) are used along with the control (AI_SI) and fully constrained (AF_SF) experiments. ~~Because atmospheric nudging also strongly constrains land-atmosphere interactions the~~ The experiment with nudged atmosphere and interactive soil moisture (AF_SI) ~~is not considered. However, strong soil moisture anomalies might also influence the circulation in some cases (e.g. Teng et al., 2019). In general, this effect is minor compared to the land reacting to atmospheric conditions and furthermore,~~ leads to similar temperature anomalies during heatwaves like the AF_SF experiment. Atmospheric nudging strongly constrains land surface conditions due to the control on available moisture and because in AF_SF ERA-Interim is used to derive the target soil moisture that is prescribed, similar land surface conditions result in both experiments. Hence, AF_SI is not considered in the disentangling procedure (see Fig. 2). To have more robust results, two disentangling approaches are considered ~~as in Wehrli et al. (2019) to have more robust results like in Wehrli et al. (2019).~~ Both approaches tend to produce similar results indicating that in a first order assumption the contributions can be treated as additive. Nevertheless, it has to be noted that disentangling causality in a coupled system always comes with limitations. Differences between the approaches show nonlinearities in the responses due to feedbacks.

TX anomalies during four recent heatwaves are attributed to their physical drivers and to climate change. The four events considered are: the 2010 Russian heatwave, the 2012 heatwave in the ~~Midwest of the United States~~ U.S., the Australian heatwave of 2012/2013 and the European heatwave in 2015. Overall the models show good agreement on the role of the drivers. Recent warming (since 1982–2008) is found to positively contribute to the event anomaly for all events and nearly all models (not for the Australian heatwave 2012/2013 and EC-Earth). The largest contribution is found for the ~~Midwest-U.S.~~ heatwave 2012 (15%–23%) and for the European heatwave 2015, however for the latter event the three models agree less on the relative role of climate change (12%–34%). ~~The~~ In the presented setup the ocean was not found to have a substantial role in driving any of the events considered. This could be due to the limited interaction between the ocean and the atmosphere due to the prescription of SSTs and sea ice or because the ocean was indeed not a driver of the events considered. For the Australian heatwave 2012/2013, the ocean is found to influence the temperature anomaly negatively in CESM (-23%). This is in accordance with the cool to neutral phase of the El Niño Southern Oscillation (NOAA Climate Prediction Center, 2022). For all four heatwaves the models show that both atmospheric circulation and land surface conditions significantly contribute to the event anomaly. For the Russian heatwave 2010 and the European heatwave 2015, atmospheric circulation is the dominant driver with land surface conditions playing a secondary but still important role. Yet, for the ~~Midwest-U.S.~~ heatwave 2012, soil moisture is about as important as atmospheric circulation and for the Australian heatwave 2012/2013, one model shows that soil moisture is the most important driving factor and the other two models show that the two physical drivers are about equally important. Note that, by design, the ExtremeX framework does not give information on which of the drivers is the initial source of the heatwaves since the constraining of the model components was carried out for the whole simulation period and events were analysed using contemporaneous anomalies from the experiments.

The ExtremeX experiments also allow a general assessment of the respective contributions of circulation anomalies vs. soil moisture conditions for warm spells. The results are very similar for the three ESMs showing that the models generally agree

on the representation of extreme events and the driving processes behind these events. Warm spells of at least 3 days length are assessed grid point-wise and show that soil moisture is responsible for around one third to half of the temperature anomalies in transitional and tropical climate zones (Fig. 8). The regions identified resemble the regions of strong soil moisture-temperature coupling highlighted by Miralles et al. (2012) for observational data and Seneviratne et al. (2006) for global climate models. Both studies additionally identify southern Europe and Eurasia as regions of strong soil moisture-temperature coupling which is, however, not confirmed from the results presented here. Nevertheless, in regions where spells of at least two weeks can occur – like in Eurasia – soil moisture is more important for these longer events than for shorter events, driving up to one third of the temperature anomaly.

This study expands the mechanistic analysis of recent heatwaves by Wehrli et al. (2019) using three Earth System Models. The results for warm spells at the grid point level and for the four heatwaves suggest that both circulation patterns and soil moisture anomalies substantially contribute to the occurrence of heat extremes, which is consistent with Wehrli et al. (2019). Soil moisture effects are particularly important in the tropics, monsoon regions, and the US Great Plains, while circulation anomalies tend to dominate in other regions of the extratropics. These results can help to shed light on processes that need to be better taken into account in weather predictions and climate projections. For instance, the important role of soil moisture conditions for extremes suggests that soil moisture monitoring and initialization could substantially ~~help improve weather prediction of~~ improve forecasting of weather extremes in several regions.

Data availability. Simulation data from the models is available from https://data.iac.ethz.ch/Wehrli_et_al_2022_ExtremeX/

555 *Author contributions.* KW, MH and SIS designed the experiments with input from OM and RV. FL ran the EC-Earth3 simulations with technical help from FS, WM and PLS. HS ran the interactive and atmosphere nudged simulations with MIROC5. DT and HK ran the soil moisture nudged simulations with MIROC5. KW ran the CESM1.2 model simulations with technical support by MH. KW analysed the results from all models. KW, FL, MH, HS, DT, HK, DC, WM, OM, RV and SIS contributed to the discussion of results. KW prepared the manuscript with contributions from all co-authors.

560 *Competing interests.* The authors declare that they have no conflict of interest.

Acknowledgements. MIROC5 simulations were contributed by NIES Japan and University of Tokyo. EC-Earth3 simulations were contributed by VU Amsterdam and KNMI. CESM1.2 simulations were contributed by ETH Zurich. [The authors thank Paul Dirmeyer and one anonymous reviewer for their valuable comments and suggestions to the manuscript. The authors also thank Dominik Schumacher for his feedback on the revised manuscript.](#) KW and SIS acknowledge funding from the European Research Council (ERC) (“DROUGHT-HEAT” project, Grant 617518). FL, DC and FS acknowledge VIDI-award from Netherlands Organisation for Scientific Research (NWO) (Persistent Summer Extremes “PERSIST” project). HS was supported by the Integrated Research Program for Advancing Climate Models (JPMXD0717935457). [HK acknowledges the National Research Foundation of Korea \(NRF\) grant funded by the Korea Government \(MSIT\)\(2021H1D3A2A03097768 and NRF-2018R1A5A7025409\).](#) WM is supported through the Swedish strategic research area Modelling the Regional and Global Earth system (MERGE). The MIROC5 simulations were performed by using Earth Simulator in JAMSTEC and the NEC SX in NIES. KW, MH and SIS acknowledge the support of Matthieu Leclair and Benoit P. Guillod in the design of the experiments and advice during the course of the project. This study uses the LandFlux–EVAL merged benchmark synthesis products of ETH Zurich produced under the aegis of the GEWEX and ILEAPS projects (<http://www.iac.ethz.ch/url/research/LandFlux-EVAL/>).

565
570

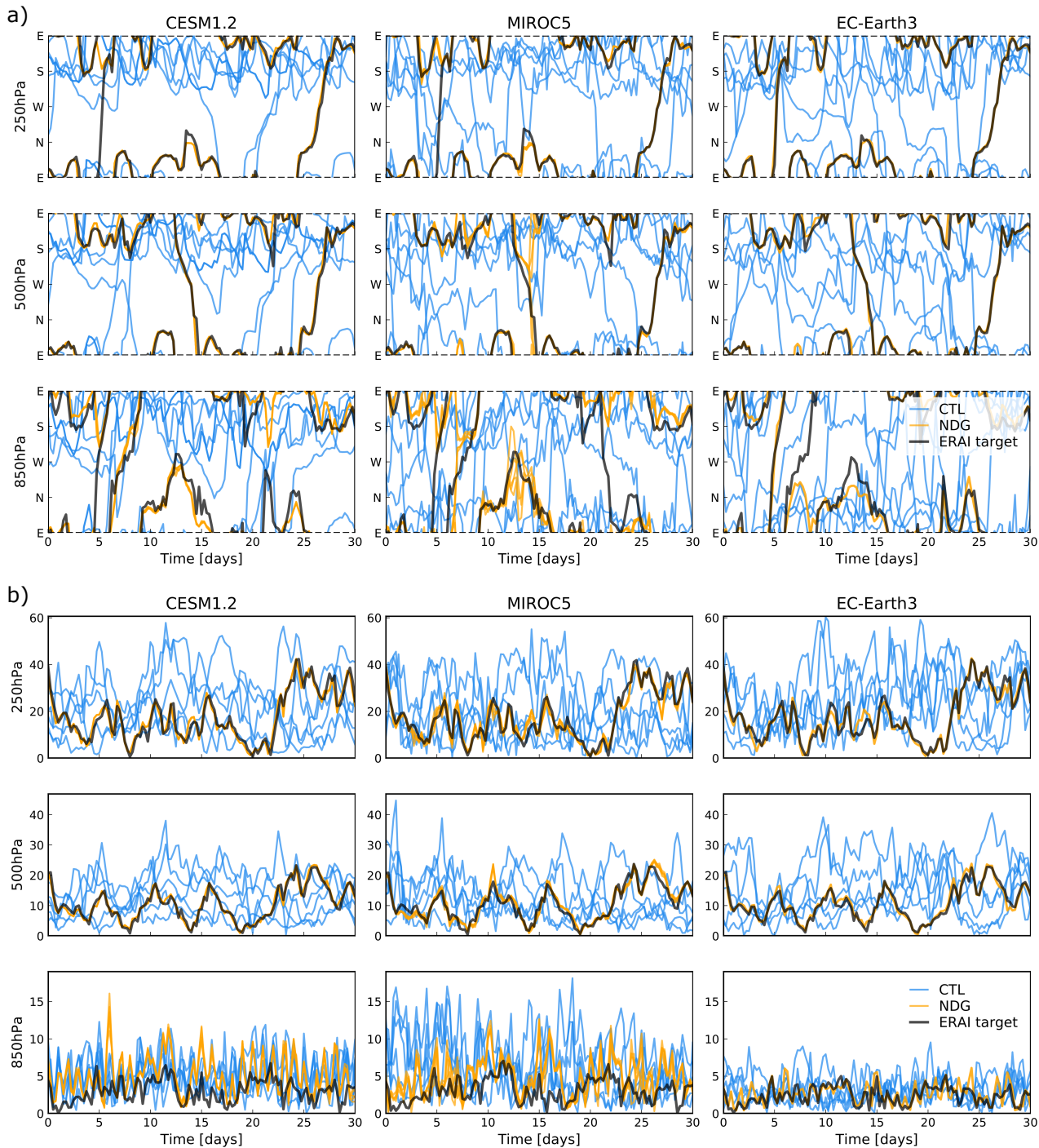


Figure A1. Comparison of winds for the experiments with nudged atmosphere (NDG, corresponds to AF_SI) and free atmosphere (CTL, corresponds to AI_SI). Shown are 6-hourly wind direction (a) and wind speed (b) during one month (June 2000) for one grid point over the Alps. The winds from the models were interpolated to 250 hPa, 500 hPa and 850 hPa. The winds from ERA-Interim (ERA-Interim) were interpolated to the same pressure levels and the model resolution for each model.

U, V @500hPa and @850hPa biases June 2000 compared to ERA-Interim

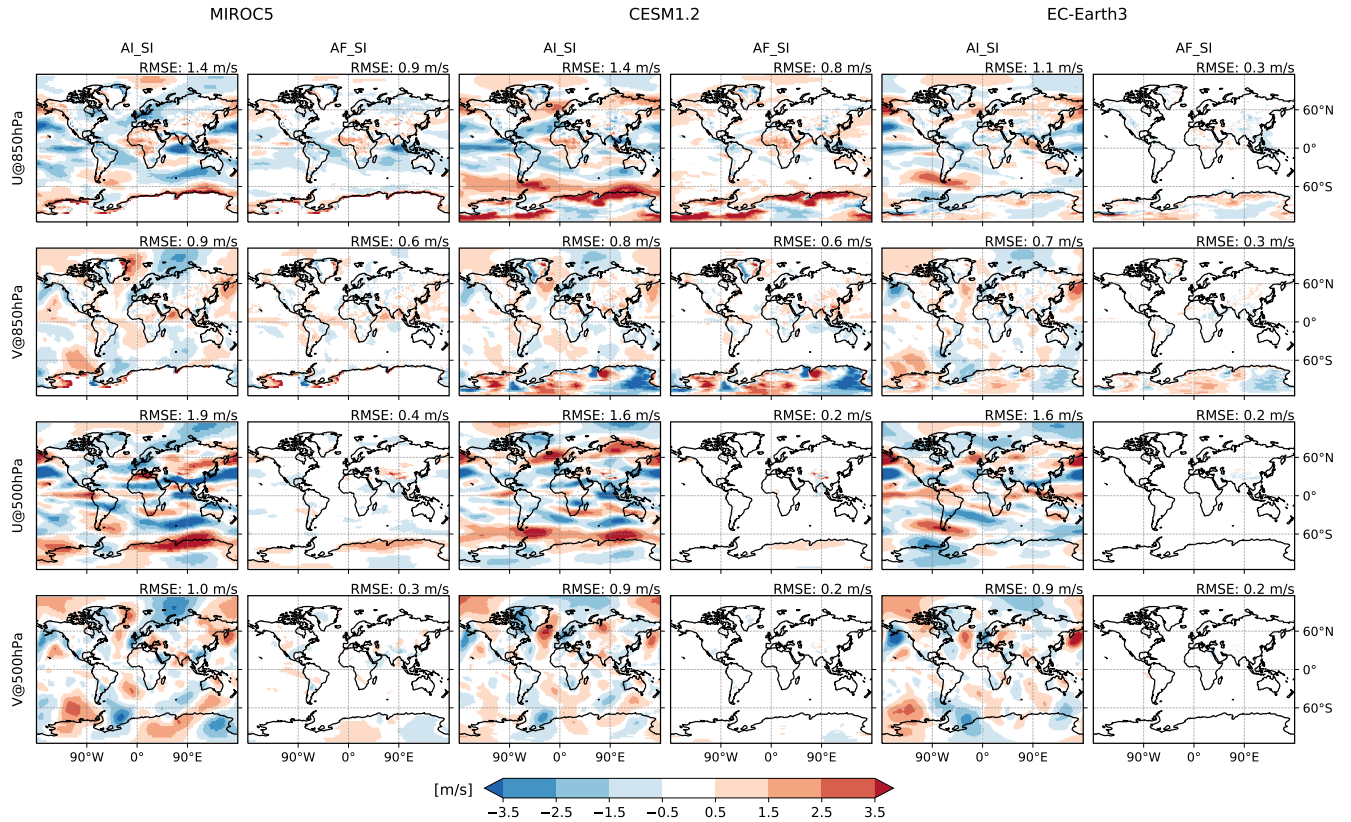
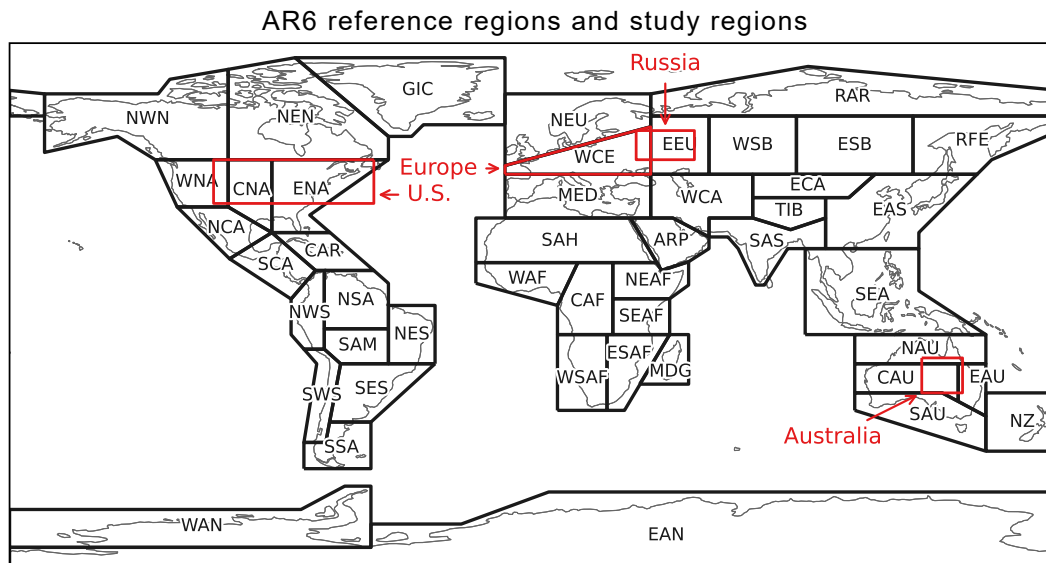


Figure A2. Bias of the zonal (U) and meridional (V) wind components at 850hPa and 500hPa for the experiments with nudged atmosphere (AF_SI) and free atmosphere (AI_SI), showing the ensemble mean where multiple simulations are available. Shown is the average over 6-hourly wind fields for one month (June 2000). The winds from the models were interpolated to 500 hPa and 850 hPa. The winds from ERA-Interim were interpolated to the same pressure levels and the model resolution for each model.



Abbrev.	Name	Abbrev.	Name	Abbrev.	Name
GIC	Greenland/Iceland	NEU	N.Europe	RFE	Russian-Far-East
NWN	N.W.North-America	WCE	West&Central-Europe	WCA	W.C.Asia
NEN	N.E.North-America	EEU	E.Europe	ECA	E.C.Asia
WNA	W.North-America	MED	Mediterranean	TIB	Tibetan-Plateau
CNA	C.North-America	SAH	Sahara	EAS	E.Asia
ENA	E.North-America	WAF	Western-Africa	ARP	Arabian-Peninsula
NCA	N.Central-America	CAF	Central-Africa	SAS	S.Asia
SCA	S.Central-America	NEAF	N.Eastern-Africa	SEA	S.E.Asia
CAR	Caribbean	SEAF	S.Eastern-Africa	NAU	N.Australia
NWS	N.W.South-America	WSAF	W.Southern-Africa	CAU	C.Australia
NSA	N.South-America	ESAF	E.Southern-Africa	EAU	E.Australia
NES	N.E.South-America	MDG	Madagascar	SAU	S.Australia
SAM	South-American-Monsoon	RAR	Russian-Arctic	NZ	New-Zealand
SWS	S.W.South-America	WSB	W.Siberia	EAN	E.Antarctica
SES	S.E.South-America	ESB	E.Siberia	WAN	W.Antarctica
SSA	S.South-America				

Figure A3. Reference regions of the IPCC AR6 as defined in Iturbide et al. (2020). [The event regions used in Sect. 5.1 are indicated in red.](#)

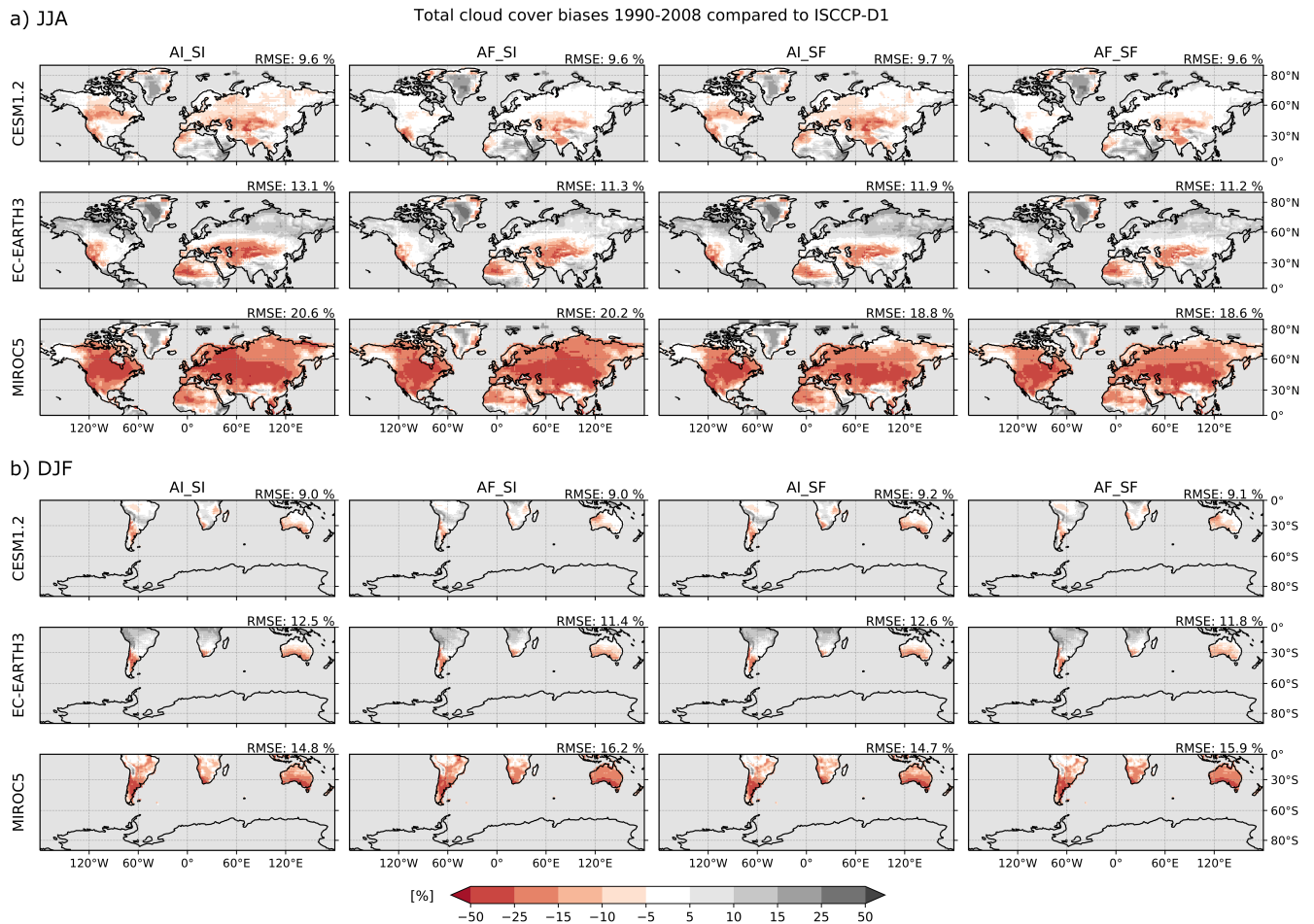


Figure A4. Bias in total cloud cover with respect to ISCCP-D1. Average over (a) JJA for the June-July-August season Northern Hemisphere and (b) DJF for the Southern Hemisphere. Ocean grid points and Antarctica are masked out. The RMSE averaged over all valid grid points of the respective hemisphere is given in mm per day in the upper right corner of each experiment and model.

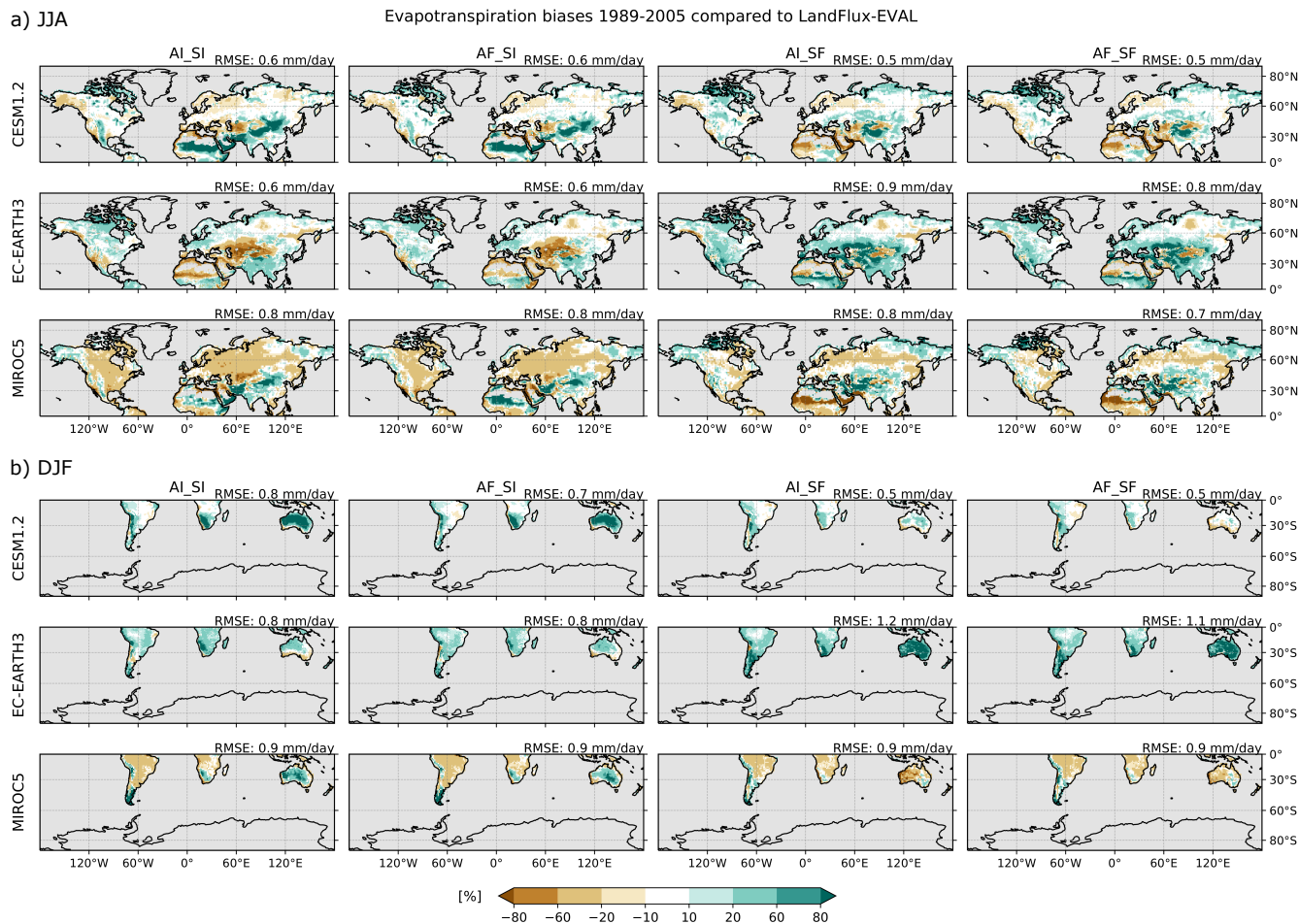
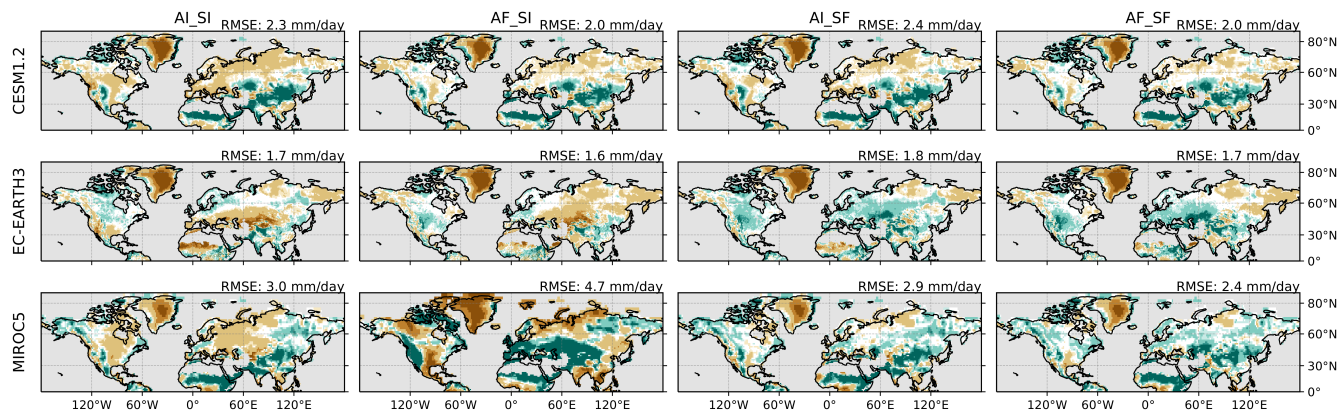


Figure A5. Bias in evapotranspiration with respect to LandFlux-Eval. Average over (a) JJA for the June-July-August season Northern Hemisphere and (b) DJF for the Southern Hemisphere. Masked out are grid points with a seasonal average of less than 0.1 mm evapotranspiration per day in the reference data set. Additionally, ocean grid points, grid points north of 75°N, Antarctica, Greenland and Iceland are masked out using the Greenland/Iceland (“GIC”) region from the AR6 reference regions for the latter two. The RMSE averaged over all valid grid points of the respective hemisphere is given in mm per day in the upper right corner of each experiment and model.

a) JJA

Precipitation biases 1982-2008 compared to MSWEP



b) DJF

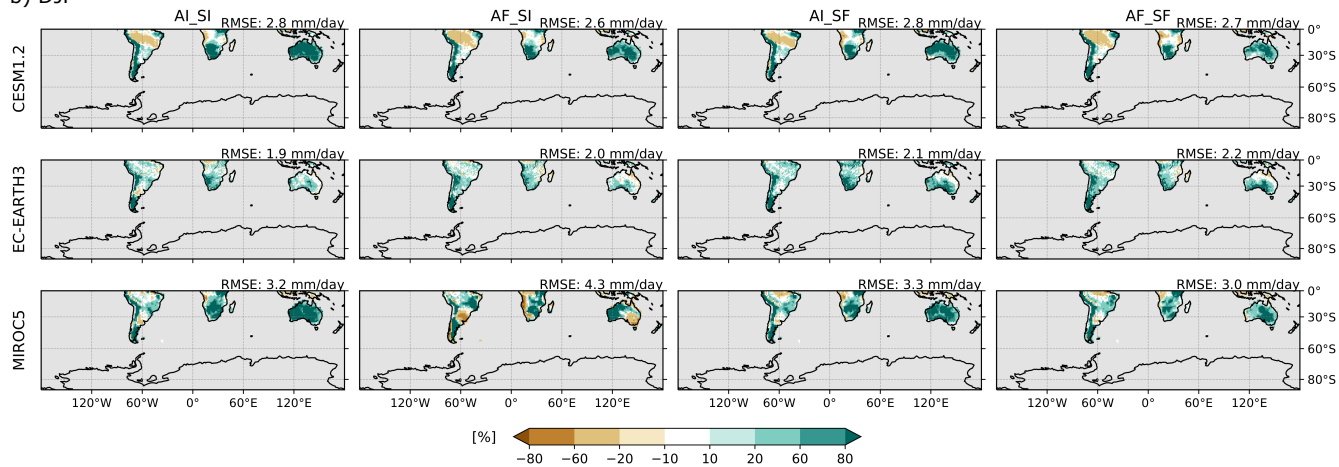


Figure A6. Same as Fig. 5 but using MSWEP as reference data set.

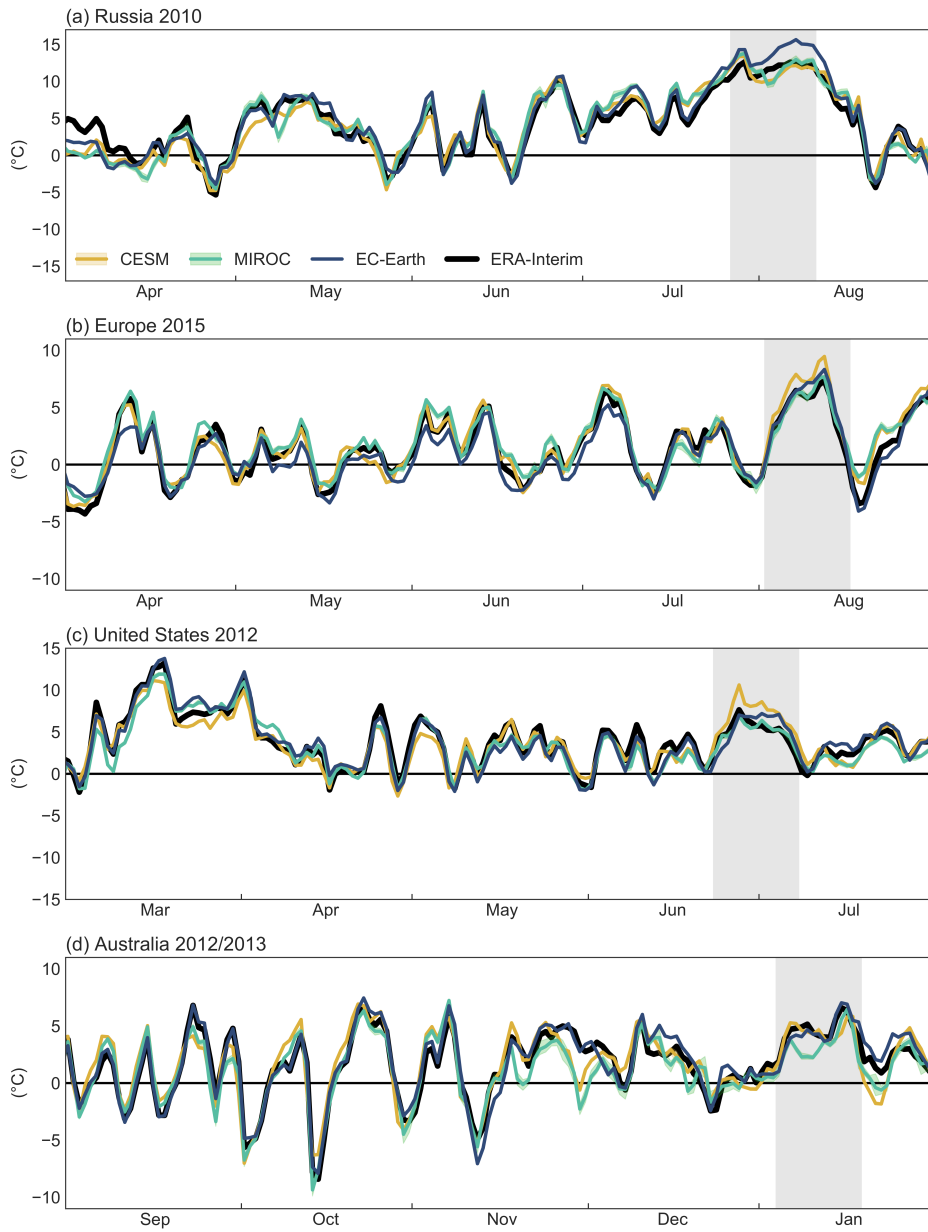


Figure A7. Same as Fig. 6 but for the nudging experiment (AF_SJ). The shading shows the full ensemble spread and lines the ensemble mean (or single simulation for EC-Earth).

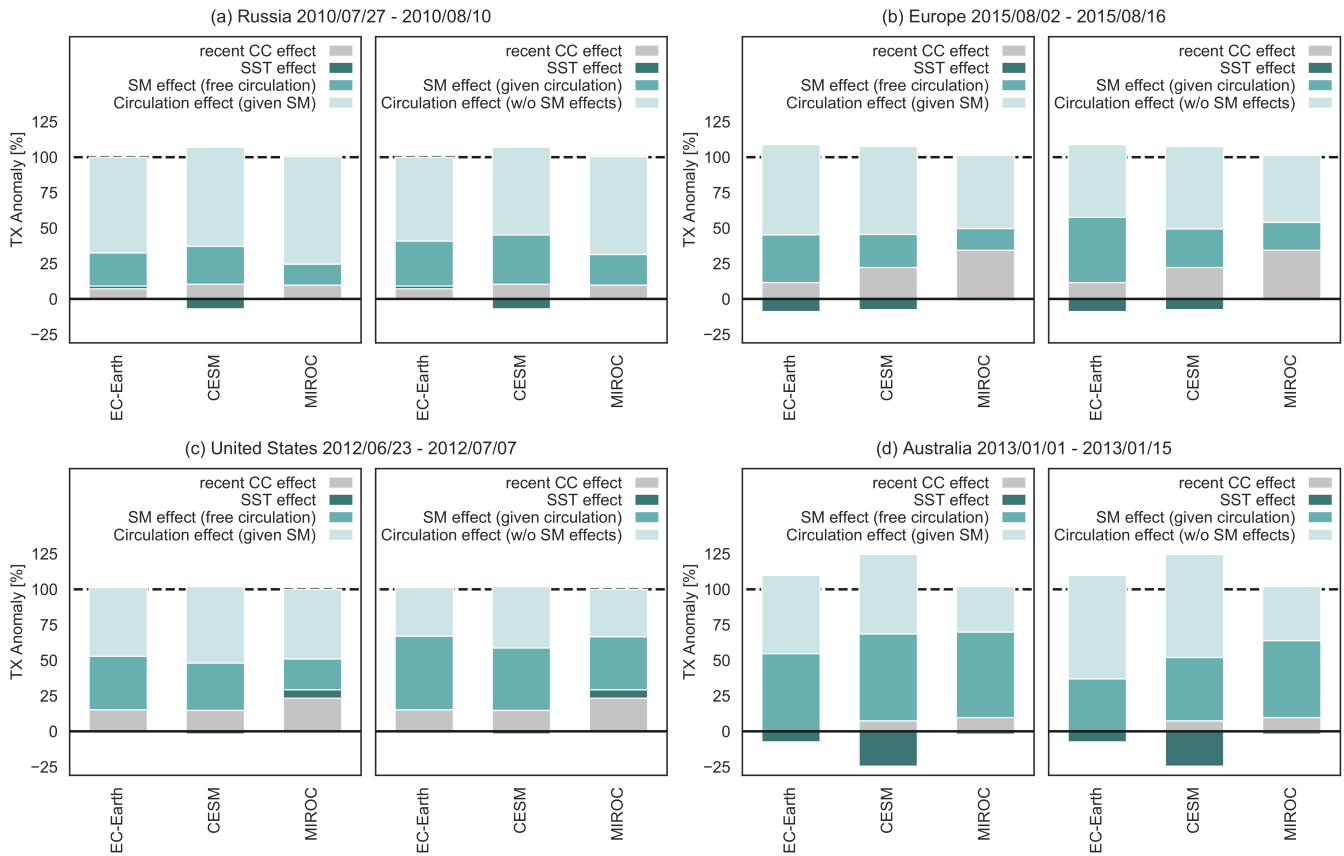


Figure A8. Same as Fig. 7 but showing the separate effects for the two approaches to compute SM vs. ATM contributions (left A, right B).

References

- Angélil, O., Perkins-Kirkpatrick, S., Alexander, L. V., Stone, D., Donat, M. G., Wehner, M., Shiogama, H., Ciavarella, A., and Christidis, N.:
575 Comparing regional precipitation and temperature extremes in climate model and reanalysis products, *Weather and Climate Extremes*, 13,
35–43, <https://doi.org/10.1016/j.wace.2016.07.001>, 2016.
- Arblaster, J. M., Lim, E.-P., Hendon, H. H., Trewin, B. C., Wheeler, M. C., Liu, G., and Braganza, K.: Understanding Australia’s hottest
September on record, *Bulletin of the American Meteorological Society*, 95, 37–41, <https://doi.org/10.1175/1520-0477-95.9.S1.1>, 2014.
- Balsamo, G., Beljaars, A., Scipal, K., Viterbo, P., van den Hurk, B., Hirschi, M., and Betts, A. K.: A revised hydrology for the ECMWF
580 model: verification from field site to terrestrial water storage and impact in the integrated forecast system, *Journal of Hydrometeorology*,
10, 623–643, <https://doi.org/10.1175/2008JHM1068.1>, 2009.
- Balsamo, G., Albergel, C., Beljaars, A., Boussetta, S., Brun, E., Cloke, H., Dee, D., Dutra, E., Muñoz Sabater, J., Pappenberger, F., de Rosnay,
P., Stockdale, T., and Vitart, F.: ERA-Interim/Land: a global land surface reanalysis data set, *Hydrology and Earth System Sciences*, 19,
389–407, <https://doi.org/10.5194/hess-19-389-2015>, 2015.
- 585 Barriopedro, D., Fischer, E. M., Luterbacher, J., Trigo, R. M., and García-Herrera, R.: The hot summer of 2010: Redrawing the temperature
record map of Europe, *Science*, 332, 220–224, <https://doi.org/10.1126/science.1201224>, 2011.
- Beck, H. E., Wood, E. F., Pan, M., Fisher, C. K., Miralles, D. G., van Dijk, A. I. J. M., McVicar, T. R., and Adler, R. F.: MSWEP
V2 global 3-hourly 0.1° precipitation: methodology and quantitative assessment, *Bulletin of the American Meteorological Society*,
<https://doi.org/10.1175/BAMS-D-17-0138.1>, 2018.
- 590 Bony, S., Stevens, B., Frierson, D. M. W., Jakob, C., Kageyama, M., Pincus, R., Shepherd, T. G., Sherwood, S. C., Siebesma,
A. P., Sobel, A. H., Watanabe, M., and Webb, M. J.: Clouds, circulation and climate sensitivity, *Nature Geoscience*, 8, 261–268,
<https://doi.org/10.1038/ngeo2398>, 2015.
- Bureau of Meteorology: Extreme heat and fire weather in December 2019 and January 2020, *Spec. Clim. Statement*, 73 (available through:
<http://www.bom.gov.au/climate/current/statements/scs73.pdf>), 2020.
- 595 Dee, D. P., Uppala, S. M., Simmons, A. J., Berrisford, P., Poli, P., Kobayashi, S., Andrae, U., Balmaseda, M. A., Balsamo, G., Bauer,
P., Bechtold, P., Beljaars, A. C. M., van de Berg, L., Bidlot, J., Bormann, N., Delsol, C., Dragani, R., Fuentes, M., Geer, A. J., Haim-
berger, L., Healy, S. B., Hersbach, H., Hólm, E. V., Isaksen, I., Kållberg, P., Köhler, M., Matricardi, M., McNally, A. P., Monge-Sanz,
B. M., Morcrette, J.-J., Park, B.-K., Peubey, C., de Rosnay, P., Tavolato, C., Thépaut, J.-N., and Vitart, F.: The ERA-Interim reanalysis:
configuration and performance of the data assimilation system, *Quarterly Journal of the Royal Meteorological Society*, 137, 553–597,
600 <https://doi.org/10.1002/qj.828>, 2011.
- Dirmeyer, P. A., Balsamo, G., Blyth, E. M., Morrison, R., and Cooper, H. M.: Land-Atmosphere Interactions Exacerbated the Drought and
Heatwave Over Northern Europe During Summer 2018, *AGU Advances*, 2, e2020AV000283, <https://doi.org/10.1029/2020AV000283>,
2021.
- Dole, R., Hoerling, M., Perlwitz, J., Eischeid, J., Pegion, P., Zhang, T., Quan, X.-W., Xu, T., and Murray, D.: Was there a basis for anticipating
605 the 2010 Russian heat wave?, *Geophysical Research Letters*, 38, <https://doi.org/10.1029/2010GL046582>, 2011.
- Dole, R., Hoerling, M., Kumar, A., Eischeid, J., Perlwitz, J., Quan, X.-W., Kiladis, G., Webb, R., Murray, D., Chen, M., Wolter, K., and
Zhang, T.: The making of an extreme event: putting the pieces together, *Bulletin of the American Meteorological Society*, 95, 427–440,
<https://doi.org/10.1175/BAMS-D-12-00069.1>, 2014.

- Dong, B., Sutton, R., Shaffrey, L., and Wilcox, L.: The 2015 European heat wave, *Bulletin of the American Meteorological Society*, 97, 610 57–62, <https://doi.org/10.1175/BAMS-D-16-0140.1>, 2016.
- Döscher, R., Acosta, M., Alessandri, A., Anthoni, P., Arneth, A., Arsouze, T., Bergmann, T., Bernadello, R., Bousetta, S., Caron, L.-P., Carver, G., Castrillo, M., Catalano, F., Cvijanovic, I., Davini, P., Dekker, E., Doblas-Reyes, F. J., Docquier, D., Echevarria, P., Fladrich, U., Fuentes-Franco, R., Gröger, M., v. Hardenberg, J., Hieronymus, J., Karami, M. P., Keskinen, J.-P., Koenigk, T., Makkonen, R., Massonnet, F., Ménégos, M., Miller, P. A., Moreno-Chamarro, E., Nieradzik, L., van Noije, T., Nolan, P., O'Donnell, D., Ollinaho, P., van den Oord, 615 G., Ortega, P., Prims, O. T., Ramos, A., Reerink, T., Rousset, C., Ruprich-Robert, Y., Le Sager, P., Schmith, T., Schrödner, R., Serva, F., Sicardi, V., Sloth Madsen, M., Smith, B., Tian, T., Tourigny, E., Uotila, P., Vancoppenolle, M., Wang, S., Wårlind, D., Willén, U., Wyser, K., Yang, S., Yepes-Arbós, X., and Zhang, Q.: The EC-Earth3 Earth System Model for the Climate Model Intercomparison Project 6, *Geoscientific Model Development Discussions*, pp. 1–90, <https://doi.org/10.5194/gmd-2020-446>, 2021.
- Duchez, A., Frajka-Williams, E., Josey, S. A., Evans, D. G., Grist, J. P., Marsh, R., McCarthy, G. D., Sinha, B., Berry, D. I., and Hirschi, 620 J. J.-M.: Drivers of exceptionally cold North Atlantic ocean temperatures and their link to the 2015 European heat wave, *Environmental Research Letters*, 11, <https://doi.org/10.1088/1748-9326/11/7/074004>, 2016.
- Fischer, E. M., Seneviratne, S. I., Vidale, P. L., Lüthi, D., and Schär, C.: Soil moisture-atmosphere interactions during the 2003 European Summer heat wave, *Journal of Climate*, 20, 5081–5099, <https://doi.org/10.1175/JCLI4288.1>, 2007.
- Flato, G., Marotzke, J., Abiodun, B., Braconnot, P., Chou, S., Collins, W., Cox, P., Driouech, F., Emori, S., Eyring, V., Forest, C., Gleckler, 625 P., Guilyardi, E., Jakob, C., Kattsov, V., Reason, C., and Rummukainen, M.: Evaluation of climate models, book section 9, pp. 741–866, Cambridge University Press, Cambridge, United Kingdom and New York, NY, USA, <https://doi.org/10.1017/CBO9781107415324.020>, 2013.
- Guilod, B. P., Orlowsky, B., Miralles, D. G., Teuling, A. J., and Seneviratne, S. I.: Reconciling spatial and temporal soil moisture effects on afternoon rainfall, *Nature Communications*, 6, <https://doi.org/10.1038/ncomms7443>, 2015.
- 630 Harris, I., Osborn, T. J., Jones, P., and Lister, D.: Version 4 of the CRU TS monthly high-resolution gridded multivariate climate dataset, *Scientific Data*, 7, <https://doi.org/10.1038/s41597-020-0453-3>, 2020.
- Hauser, M., Orth, R., and Seneviratne, S. I.: Role of soil moisture versus recent climate change for the 2010 heat wave in western Russia, *Geophysical Research Letters*, 43, 2819–2826, <https://doi.org/10.1002/2016GL068036>, 2016.
- Hauser, M., Gudmundsson, L., Orth, R., Jézéquel, A., Haustein, K., Vautard, R., van Oldenborgh, G. J., Wilcox, L., and Seneviratne, S. I.: Methods and model dependency of extreme event attribution: the 2015 European drought, *Earth's Future*, 5, 1034–1043, 635 <https://doi.org/10.1002/2017EF000612>, 2017a.
- Hauser, M., Orth, R., and Seneviratne, S. I.: Investigating soil moisture–climate interactions with prescribed soil moisture experiments: An assessment with the Community Earth System Model (version 1.2), *Geoscientific Model Development*, 10, 1665–1677, <https://doi.org/10.5194/gmd-10-1665-2017>, 2017b.
- 640 Hirschi, M., Seneviratne, S. I., Alexandrov, V., Boberg, F., Boroneant, C., Christensen, O. B., Formayer, H., Orlowsky, B., and Stepanek, P.: Observational evidence for soil-moisture impact on hot extremes in southeastern Europe, *Nature Geosci*, 4, 17–21, <https://doi.org/10.1038/ngeo1032>, 2011.
- Hoerling, M., Eischeid, J., Kumar, A., Leung, R., Mariotti, A., Mo, K., Schubert, S. D., and Seager, R.: Causes and predictability of the 2012 Great Plains drought, *Bulletin of the American Meteorological Society*, 95, 269–282, <https://doi.org/10.1175/BAMS-D-13-00055.1>, 2014.
- 645 Hope, P., Wang, G., Lim, E.-P., Hendon, H. H., and Arblaster, J. M.: What caused the record-breaking heat across Australia in October 2015?, *Bulletin of the American Meteorological Society*, 97, 122–126, <https://doi.org/10.1175/BAMS-D-16-0141.1>, 2016.

- Hurrell, J. W., Hack, J. J., Shea, D., Caron, J. M., and Rosinski, J.: A new sea surface temperature and sea ice boundary dataset for the Community Atmosphere Model, *Journal of Climate*, 21, 5145–5153, <https://doi.org/10.1175/2008JCLI2292.1>, 2008.
- 650 Hurrell, J. W., Holland, M. M., Gent, P. R., Ghan, S., Kay, J. E., Kushner, P. J., Lamarque, J.-F., Large, W. G., Lawrence, D., Lindsay, K., Lipscomb, W. H., Long, M. C., Mahowald, N., Marsh, D. R., Neale, R. B., Rasch, P., Vavrus, S., Vertenstein, M., Bader, D., Collins, W. D., Hack, J. J., Kiehl, J., and Marshall, S.: The Community Earth System Model: a framework for collaborative research, *Bulletin of the American Meteorological Society*, 94, 1339–1360, <https://doi.org/10.1175/BAMS-D-12-00121.1>, 2013.
- Iturbide, M., Gutiérrez, J. M., Alves, L. M., Bedia, J., Cerezo-Mota, R., Gimpeanu, E., Goni, A. S., Di Luca, A., Faria, S. H., Gorodetskaya, I. V., Hauser, M., Herrera, S., Hennessy, K., Hewitt, H. T., Jones, R. G., Krakovska, S., Manzananas, R., Martínez-Castro, D., 655 Narisma, G. T., Nurhati, I. S., Pinto, I., Seneviratne, S. I., van den Hurk, B., and Vera, C. S.: An update of IPCC climate reference regions for subcontinental analysis of climate model data: Definition and aggregated datasets, *Earth System Science Data*, 12, 2959–2970, <https://doi.org/10.5194/essd-12-2959-2020>, 2020.
- Jaeger, E. B. and Seneviratne, S. I.: Impact of soil moisture-atmosphere coupling on European climate extremes and trends in a regional climate model, *Climate Dynamics*, 36, 1919–1939, <https://doi.org/10.1007/s00382-010-0780-8>, 2011.
- 660 Jeuken, A. B. M., Siegmund, P. C., Heijboer, L. C., Feichter, J., and Bengtsson, L.: On the potential of assimilating meteorological analyses in a global climate model for the purpose of model validation, *Journal of Geophysical Research: Atmospheres*, 101, 16 939–16 950, <https://doi.org/10.1029/96JD01218>, 1996.
- King, A. D., Karoly, D. J., Donat, M. G., and Alexander, L. V.: Climate change turns Australia’s 2013 big dry into a year of record-breaking heat [in "Explaining Extremes of 2013 from a Climate Perspective"], *Bulletin of the American Meteorological Society*, 95, 665 41–45, <https://doi.org/10.1175/1520-0477-95.9.S1.1>, 2014.
- Kooperman, G. J., Pritchard, M. S., Ghan, S. J., Wang, M., Somerville, R. C. J., and Russell, L. M.: Constraining the influence of natural variability to improve estimates of global aerosol indirect effects in a nudged version of the Community Atmosphere Model 5, *Journal of Geophysical Research: Atmospheres*, 117, <https://doi.org/10.1029/2012JD018588>, d23204, 2012.
- Koster, R. D., Dirmeyer, P. A., Guo, Z., Bonan, G., Chan, E., Cox, P., Gordon, C. T., Kanae, S., Kowalczyk, E., Lawrence, D., Liu, P., 670 Lu, C.-H., Malyshev, S., McAvaney, B., Mitchell, K., Mocko, D., Oki, T., Oleson, K., Pitman, A., Sud, Y. C., Taylor, C. M., Verseghy, D., Vasic, R., Xue, Y., and Yamada, T.: Regions of strong coupling between soil moisture and precipitation, *Science*, 305, 1138–1140, <https://doi.org/10.1126/science.1100217>, 2004.
- Koster, R. D., Guo, Z., Yang, R., Dirmeyer, P. A., Mitchell, K., and Puma, M. J.: On the nature of soil moisture in land surface models, *Journal of Climate*, 22, 4322–4335, <https://doi.org/10.1175/2009JCLI2832.1>, 2009.
- 675 Kröner, N., Kotlarski, S., Fischer, E. M., Lüthi, D., Zubler, E., and Schär, C.: Separating climate change signals into thermodynamic, lapse-rate and circulation effects: theory and application to the European summer climate, *Climate Dynamics*, 48, 3425–3440, <https://doi.org/10.1007/s00382-016-3276-3>, 2017.
- Lawrence, D. M., Oleson, K. W., Flanner, M. G., Thornton, P. E., Swenson, S. C., Lawrence, P. J., Zeng, X., Yang, Z.-L., Levis, S., Sakaguchi, K., Bonan, G. B., and Slater, A. G.: Parameterization improvements and functional and structural advances in version 4 of the Community 680 Land Model, *Journal of Advances in Modeling Earth Systems*, 3, <https://doi.org/10.1029/2011MS00045>, 2011.
- Lewis, S. C. and Karoly, D. J.: Anthropogenic contributions to Australia’s record summer temperatures of 2013, *Geophysical Research Letters*, 40, 3705–3709, <https://doi.org/10.1002/grl.50673>, 2013.

- Maraun, D., Shepherd, T. G., Widmann, M., Zappa, G., Walton, D., Gutiérrez, J., Hagemann, S., Richter, I., Soares, P. M. M., Hall, A., and Mearns, L. O.: Towards process-informed bias correction of climate change simulations, *Nature Climate Change*, 7, 764–773, <https://doi.org/10.1038/nclimate3418>, 2017.
- Martius, O., Sodemann, H., Joos, H., Pfahl, S., Winschall, A., Croci-Maspoli, M., Graf, M., Madonna, E., Mueller, B., Schemm, S., Sedláček, J., Sprenger, M., and Wernli, H.: The role of upper-level dynamics and surface processes for the Pakistan flood of July 2010, *Quarterly Journal of the Royal Meteorological Society*, 139, 1780–1797, <https://doi.org/10.1002/qj.2082>, 2012.
- Mauritsen, T., Stevens, B., Roeckner, E., Crueger, T., Esch, M., Giorgetta, M., Haak, H., Jungclaus, J., Klocke, D., Matei, D., Mikolajewicz, U., Notz, D., Pincus, R., Schmidt, H., and Tomassini, L.: Tuning the climate of a global model, *Journal of Advances in Modeling Earth Systems*, 4, <https://doi.org/10.1029/2012MS000154>, 2012.
- Meinshausen, M., Nicholls, Z. R. J., Lewis, J., Gidden, M. J., Vogel, E., Freund, M., Beyerle, U., Gessner, C., Nauels, A., Bauer, N., Canadell, J. G., Daniel, J. S., John, A., Krummel, P. B., Luderer, G., Meinshausen, N., Montzka, S. A., Rayner, P. J., Reimann, S., Smith, S. J., van den Berg, M., Velders, G. J. M., Vollmer, M. K., and Wang, R. H. J.: The shared socio-economic pathway (SSP) greenhouse gas concentrations and their extensions to 2500, *Geoscientific Model Development*, 13, 3571–3605, <https://doi.org/10.5194/gmd-13-3571-2020>, 2020.
- Merz, B., Kuhlicke, C., Kunz, M., Pittore, M., Babeyko, A., Bresch, D. N., Domeisen, D. I. V., Feser, F., Koszalka, I., Kreibich, H., Pantillon, F., Parolai, S., Pinto, J. G., Punge, H. J., Rivalta, E., Schröter, K., Strehlow, K., Weisse, R., and Wurpts, A.: Impact forecasting to support emergency management of natural hazards, *Reviews of Geophysics*, 58, e2020RG000704, <https://doi.org/10.1029/2020RG000704>, 2020.
- Miralles, D. G., van den Berg, M. J., Teuling, A. J., and de Jeu, R. A. M.: Soil moisture-temperature coupling: a multiscale observational analysis, *Geophysical Research Letters*, 39, <https://doi.org/10.1029/2012GL053703>, 2012.
- Miralles, D. G., Gentine, P., Seneviratne, S. I., and Teuling, A. J.: Land–atmospheric feedbacks during droughts and heatwaves: state of the science and current challenges, *Annals of the New York Academy of Sciences*, 1436, 19–35, <https://doi.org/10.1111/nyas.13912>, 2019.
- Moon, H., Gudmundsson, L., and Seneviratne, S. I.: Drought persistence errors in global climate models, *Journal of Geophysical Research: Atmospheres*, 123, 3483–3496, <https://doi.org/10.1002/2017JD027577>, 2018.
- Moon, H., Guillod, B. P., Gudmundsson, L., and Seneviratne, S. I.: Soil moisture effects on afternoon precipitation occurrence in current climate models, *Geophysical Research Letters*, 46, 1861–1869, <https://doi.org/10.1029/2018GL080879>, 2019.
- Mueller, B. and Seneviratne, S. I.: Systematic land climate and evapotranspiration biases in CMIP5 simulations, *Geophysical Research Letters*, 41, 128–134, <https://doi.org/10.1002/2013GL058055>, 2014.
- Mueller, B., Hirschi, M., Jimenez, C., Ciais, P., Dirmeyer, P. A., Dolman, A. J., Fisher, J. B., Jung, M., Ludwig, F., Maignan, F., Miralles, D. G., McCabe, M. F., Reichstein, M., Sheffield, J., Wang, K., Wood, E. F., Zhang, Y., and Seneviratne, S. I.: Benchmark products for land evapotranspiration: LandFlux-EVAL multi-data set synthesis, *Hydrology and Earth System Sciences*, 17, 3707–3720, <https://doi.org/10.5194/hess-17-3707-2013>, 2013.
- Neale, R. B., Chen, C.-C., Gettelman, A., Lauritzen, P. H., Park, S., Williamson, D. L., Conley, A. J., Garcia, R., Kinnison, D., Lamarque, J.-F., Marsh, D., Mills, M., Smith, A. K., Tilmes, S., Vitt, F., Morrison, H., Cameron-Smith, P., Collins, W. D., Iacono, M. J., Easter, R. C., Ghan, S. J., Liu, X., Rasch, P. J., and Taylor, M. A.: Description of the NCAR Community Atmosphere Model (CAM 5.0), Technical report, National Center for Atmospheric Research. Boulder, Colorado, 2012.
- NOAA Climate Prediction Center: Historical El Niño / La Niña episodes (1950-present) based on the Oceanic Niño Index, https://origin.cpc.ncep.noaa.gov/products/analysis_monitoring/ensostuff/ONI_v5.php, accessed 15 February 2022, 2022.
- Oleson, K. W., Lawrence, D. M., Bonan, G. B., Flanner, M. G., Kluzek, E., Lawrence, P. J., Levis, S., Swenson, S. C., Thornton, P. E., Dai, A., Decker, M., Dickinson, R., Feddema, J., Heald, C. L., Hoffman, F., Lamarque, J.-F., Mahowald, N., Niu, G.-Y., Qian, T., Randerson,

- J., Running, S., Sakaguchi, K., Slater, A., Stöckli, R., Wang, A., Yang, Z.-L., Zeng, X., and Zeng, X.: Technical description of version 4.0 of the Community Land Model (CLM), Technical report, National Center for Atmospheric Research. Boulder, Colorado, 2010.
- Orth, R., Zscheischler, J., and Seneviratne, S. I.: Record dry summer in 2015 challenges precipitation projections in Central Europe, *Scientific Reports*, 6, 28 334, <https://doi.org/10.1038/srep28334>, 2016.
- 725 PaiMazumder, D. and Done, J. M.: Potential predictability sources of the 2012 U.S. drought in observations and a regional model ensemble, *Journal of Geophysical Research: Atmospheres*, 121, 12,581–12,592, <https://doi.org/10.1002/2016JD025322>, 2016.
- Petch, J. C., Short, C. J., Best, M. J., McCarthy, M., Lewis, H. W., Vosper, S. B., and Weeks, M.: Sensitivity of the 2018 UK summer heatwave to local sea temperatures and soil moisture, *Atmospheric Science Letters*, 21, e948, <https://doi.org/https://doi.org/10.1002/asl.948>, 2020.
- Pfahl, S., O’Gorman, P. A., and Fischer, E. M.: Understanding the regional pattern of projected future changes in extreme precipitation, 730 *Nature Climate Change*, 7, 423–427, <https://doi.org/10.1038/nclimate3287>, 2017.
- Power, S. B. and Delage, F. P. D.: Setting and smashing extreme temperature records over the coming century, *Nature Climate Change*, 9, 529–534, <https://doi.org/10.1038/s41558-019-0498-5>, 2019.
- Quesada, B., Vautard, R., Yiou, P., Hirschi, M., and Seneviratne, S. I.: Asymmetric European summer heat predictability from wet and dry southern winters and springs, *Nature Climate Change*, 2, 736–741, <https://doi.org/10.1038/nclimate1536>, 2012.
- 735 Rahmstorf, S. and Coumou, D.: Increase of extreme events in a warming world, *Proceedings of the National Academy of Sciences*, 108, 17 905–17 909, <https://doi.org/10.1073/pnas.1101766108>, 2011.
- Rayner, N. A., Parker, D. E., Horton, E. B., Folland, C. K., Alexander, L. V., Rowell, D. P., Kent, E. C., and Kaplan, A.: Global analyses of sea surface temperature, sea ice, and night marine air temperature since the late nineteenth century, *Journal of Geophysical Research: Atmospheres*, 108, <https://doi.org/10.1029/2002JD002670>, 2003.
- 740 Rossow, W. B. and Schiffer, R. A.: Advances in Understanding Clouds from ISCCP, *Bulletin of the American Meteorological Society*, 80, 2261–2288, [https://doi.org/10.1175/1520-0477\(1999\)080%3C2261%3AAIUCFI%3E2.0.CO;2](https://doi.org/10.1175/1520-0477(1999)080%3C2261%3AAIUCFI%3E2.0.CO;2), 1999.
- Santanello, J. A., Dirmeyer, P. A., Ferguson, C. R., Findell, K. L., Tawfik, A. B., Berg, A., Ek, M., Gentile, P., Guillod, B. P., van Heerwaarden, C., Roundy, J., and Wulfmeyer, V.: Land-atmosphere interactions: the LoCo perspective, *Bulletin of the American Meteorological Society*, 99, 1253–1272, <https://doi.org/10.1175/BAMS-D-17-0001.1>, 2018.
- 745 Seneviratne, S. I., Lüthi, D., Litschi, M., and Schär, C.: Land-atmosphere coupling and climate change in Europe, *Nature*, 443, 205–209, <https://doi.org/10.1038/nature05095>, 2006.
- Seneviratne, S. I., Corti, T., Davin, E. L., Hirschi, M., Jaeger, E. B., Lehner, I., Orlowsky, B., and Teuling, A. J.: Investigating soil moisture-climate interactions in a changing climate: A review, *Earth-Science Reviews*, 99, 125–161, <https://doi.org/10.1016/j.earscirev.2010.02.004>, 2010.
- 750 Seneviratne, S. I., Nicholls, N., Easterling, D., Goodess, C. M., Kanae, S., Kossin, J., Luo, Y., Marengo, J., Innes, K. M., Rahimi, M., Reichstein, M., Sorteberg, A., Vera, C., Zhang, X., Rusticucci, M., Semenov, V., Alexander, L. V., Allen, S., Benito, G., Cavazos, T., Clague, J., Conway, D., Della-Marta, P. M., Gerber, M., Gong, S., Goswami, B. N., Hemer, M., Huggel, C., den Hurk, B. V., Kharin, V. V., Kitoh, A., Tank, A. M. G. K., Li, G., Mason, S., Guire, W. M., Oldenborgh, G. J. V., Orlowsky, B., Smith, S., Thiaw, W., Velegrakis, A., Yiou, P., Zhang, T., Zhou, T., and Zwiers, F. W.: Changes in climate extremes and their impacts on the natural physical environment, in: 755 *Managing the Risks of Extreme Events and Disasters to Advance Climate Change Adaptation*, pp. 109–230, edited by C. B. Field et al., Cambridge University Press, Cambridge, <https://doi.org/10.1017/CBO9781139177245.006>, 2012.
- Seneviratne, S. I., Donat, M. G., Mueller, B., and Alexander, L. V.: No pause in the increase of hot temperature extremes, *Nature Climate Change*, 4, 161–163, <https://doi.org/10.1038/nclimate2145>, 2014.

- 760 Shepherd, T. G.: Atmospheric circulation as a source of uncertainty in climate change projections, *Nature Geosci*, 7, 703–708, <https://doi.org/10.1038/ngeo2253>, 2014.
- Shiogama, H., Watanabe, M., Imada, Y., Mori, M., Ishii, M., and Kimoto, M.: An event attribution of the 2010 drouwght in the South Amazon region using the MIROC5 model, *Atmospheric Science Letters*, 14, 170–175, <https://doi.org/10.1002/asl2.435>, 2013.
- 765 Shiogama, H., Imada, Y., Mori, M., Mizuta, R., Stone, D., Yoshida, K., Arakawa, O., Ikeda, M., Takahashi, C., Arai, M., Ishii, M., Watanabe, M., and Kimoto, M.: Attributing historical changes in probabilities of record-breaking daily temperature and precipitation extreme events, *Scientific Online Letters on the Atmosphere*, 12, 225–231, 2016.
- Sillmann, J., Kharin, V. V., Zwiers, F. W., Zhang, X., and Bronaugh, D.: Climate extremes indices in the CMIP5 multimodel ensemble: Part 2. Future climate projections, *Journal of Geophysical Research: Atmospheres*, 118, 2473–2493, <https://doi.org/10.1002/jgrd.50188>, 2013.
- Suarez-Gutierrez, L., Müller, W. A., Li, C., and Marotzke, J.: Dynamical and thermodynamical drivers of variability in European summer heat extremes, *Climate Dynamics*, 54, 4351–4366, <https://doi.org/10.1007/s00382-020-05233-2>, 2020.
- 770 Takata, K., Emori, S., and Watanabe, T.: Development of the minimal advanced treatments of surface interaction and runoff, *Global and Planetary Change*, 38, 209–222, [https://doi.org/10.1016/S0921-8181\(03\)00030-4](https://doi.org/10.1016/S0921-8181(03)00030-4), 2003.
- Teng, H., Branstator, G., Tawfik, A. B., and Callaghan, P.: Circumglobal response to prescribed soil moisture over North America, *Journal of Climate*, 32, 4525–4545, <https://doi.org/10.1175/JCLI-D-18-0823.1>, 2019.
- Trenberth, K. E. and Fasullo, J. T.: Climate extremes and climate change: the Russian heat wave and other climate extremes of 2010, *Journal of Geophysical Research: Atmospheres*, 117, <https://doi.org/10.1029/2012JD018020>, 2012.
- 775 Trenberth, K. E., Fasullo, J. T., and Shepherd, T. G.: Attribution of climate extreme events, *Nature Climate Change*, 5, <https://doi.org/10.1038/nclimate2657>, 2015.
- Turner, J., Bracegirdle, T. J., Phillips, T., Marshall, G. J., and Hosking, J. S.: An initial assessment of Antarctic sea ice extent in the CMIP5 models, *Journal of Climate*, 26, 1473–1484, <https://doi.org/10.1175/JCLI-D-12-00068.1>, 2013.
- 780 van der Ent, R. J., Savenije, H. H. G., Schaefli, B., and Steele-Dunne, S. C.: Origin and fate of atmospheric moisture over continents, *Water Resources Research*, 46, <https://doi.org/10.1029/2010WR009127>, 2010.
- van Vuuren, D. P., Edmonds, J., Kainuma, M., Riahi, K., Thomson, A., Hibbard, K., Hurtt, G. C., Kram, T., Krey, V., Lamarque, J.-F., Masui, T., Meinshausen, M., Nakicenovic, N., Smith, S. J., and Rose, S. K.: The representative concentration pathways: An overview, *Climatic Change*, 109, <https://doi.org/10.1007/s10584-011-0148-z>, 2011.
- 785 Vautard, R., Yiou, P., Otto, F., Stott, P., Christidis, N., van Oldenborgh, G. J., and Schaller, N.: Attribution of human-induced dynamical and thermodynamical contributions in extreme weather events, *Environmental Research Letters*, 11, 114 009, <https://doi.org/10.1088/1748-9326/11/11/114009>, 2016.
- Wang, C., Zhang, L., Lee, S.-K., Wu, L., and Mechoso, C. R.: A global perspective on CMIP5 climate model biases, *Nature Clim. Change*, 4, 201–205, <https://doi.org/10.1038/nclimate2118>, 2014a.
- 790 Wang, G., Hope, P., Lim, E.-P., Hendon, H. H., and Arblaster, J. M.: Three methods for the attribution of extreme weather and climate events, Research Report 018 (available through: <http://www.bom.gov.au/research/publications/researchreports/BRR-018.pdf>), Bureau of Meteorology, <http://www.bom.gov.au/research/publications/researchreports/BRR-018.pdf>, 2016.
- Wang, H., Schubert, S. D., Koster, R., Ham, Y.-G., and Suarez, M.: On the role of SST forcing in the 2011 and 2012 extreme U.S. heat and drought: a study in contrasts, *Journal of Hydrometeorology*, 15, 1255–1273, <https://doi.org/10.1175/JHM-D-13-069.1>, 2014b.

- 795 Watanabe, M., Suzuki, T., O'ishi, R., Komuro, Y., Watanabe, S., Emori, S., Takemura, T., Chikira, M., Ogura, T., Sekiguchi, M., Takata, K., Yamazaki, D., Yokohata, T., Nozawa, T., Hasumi, H., Tatebe, H., and Kimoto, M.: Improved climate simulation by MIROC5: mean states, variability, and climate sensitivity, *Journal of Climate*, 23, 6312–6335, <https://doi.org/10.1175/2010JCLI3679.1>, 2010.
- Wehrli, K., Guillod, B. P., Hauser, M., Leclair, M., and Seneviratne, S. I.: Assessing the dynamic versus thermodynamic origin of climate model biases, *Geophysical Research Letters*, 45, 8471–8479, <https://doi.org/10.1029/2018GL079220>, 2018.
- 800 Wehrli, K., Guillod, B. P., Hauser, M., Leclair, M., and Seneviratne, S. I.: Identifying key driving processes of major recent heat waves, *Journal of Geophysical Research: Atmospheres*, 124, 11 746–11 765, <https://doi.org/10.1029/2019JD030635>, 2019.
- Wehrli, K., Hauser, M., and Seneviratne, S. I.: Storylines of the 2018 Northern Hemisphere heatwave at pre-industrial and higher global warming levels, *Earth System Dynamics*, 11, 855–873, <https://doi.org/10.5194/esd-11-855-2020>, 2020.
- Zappa, G., Shaffrey, L. C., and Hodges, K. I.: The ability of CMIP5 models to simulate North Atlantic extratropical cyclones, *Journal of*
805 *Climate*, 26, 5379–5396, <https://doi.org/10.1175/JCLI-D-12-00501.1>, 2013.
- Zappa, G., Hoskins, B. J., and Shepherd, T. G.: The dependence of wintertime Mediterranean precipitation on the atmospheric circulation response to climate change, *Environmental Research Letters*, 10, 104 012, <https://doi.org/10.1088/1748-9326/10/10/104012>, 2015.
- Ziese, M., Rauthe-Schöch, A., Becker, A., Finger, P., Meyer-Christoffer, A., and Schneider, U.: GPCP Full Data
Daily Version.2018 at 1.0°: daily land-surface precipitation from rain-gauges built on GTS-based and historic data,
810 https://doi.org/10.5676/dwd_gpcp/fd_d_v2018_100, 2018.
- Zscheischler, J. and Seneviratne, S. I.: Dependence of drivers affects risks associated with compound events, *Science Advances*, 3, <https://doi.org/10.1126/sciadv.1700263>, 2017.